Characterization of an *Arundo donax*-based composite: A solution to improve indoor comfort

Eleonora Cintura [a,b,*], Paulina Faria [a], Luisa Molari [c], Luca Barbaresi [d], Dario D'Orazio [d], Lina Nunes [b,e]

[a] CERIS, Department of Civil Engineering, NOVA School of Science and Technology, NOVA University of Lisbon, 2829-516 Caparica, Portugal
[b] Structures Department, National Laboratory for Civil Engineering, 1700-066 Lisbon, Portugal
[c] Department of Civil, Chemical, Environmental and Materials Engineering, DICAM, Alma Mater Studiorum - University of Bologna, 40136 Bologna, Italy
[d] Department of Industrial Engineering, DIN, Alma Mater Studiorum - University of Bologna, 40136, Bologna, Italy
[e] CE3C, Centre for Ecology, Evolution and Environmental Changes & CHANGE, Global Change and Sustainability Institute, University of the Azores, 9700-042 Angra do Heroísmo, Portugal

ARTICLE INFO

ABSTRACT

Arundo donax (giant reed or giant cane) is a widely available, perennial, invasive, non-food crop, present worldwide and employed for several uses, including building practices. Considering the increasing demand for sustainable building materials, *A. donax* can be an efficient solution. This study investigated its properties as a bio-aggregate mixed with a sodium silicate solution as an adhesive. A horizontal analysis that provided a general characterization of the composite was carried out. The results showed that the *A. donax*-based composite had an apparent density of 517 kg/m³, thermal conductivity of 0.128 W/(m.K), and high hygroscopicity, with a moisture buffering value of 4.33 g/(m² %RH), property that could be both an advantage for indoor comfort and a drawback. The uncommon sound absorption behaviour can be comparable to granular materials, with the highest sound absorption coefficient values, α, between 600 Hz and 700 Hz. Due to the range and the shape of the acoustic absorption property, this material may be helpful in acoustic treatments for speech noise. The mechanical tests defined flexural and compressive strength, respectively, 0.35 N/mm² and 0.9 N/mm², ensuring applicability. Above all, these tests opened new possible solutions for *A. donax*-based composite production either alone or in combination with other agro-industrial wastes and justified further tests, such as fire resistance and bio-susceptibility.

1. Introduction

Research is increasingly interested in the feasibility of using bio-based products for building practices, such as bio-wastes and bio-resources derived from agriculture. This solution both lowers the environmental impact caused by the construction and agriculture sectors (Ansell et al., 2020; Viel et al., 2019) and reduces the problem of solid waste disposal (Gaspar et al., 2020; Liuzzi et al., 2020b). Furthermore, it moderates the energy consumption derived from the production and use of building materials (Ntimugura et al., 2020).

Past research already addressed this topic. Cintura et al. (Cintura et al., 2021) reported many studies that considered bio-wastes and bio-resources for construction practices. Three main groups of bio-wastes were identified according to their origin: those derived from forest management and floriculture, those derived from agricultural and manufacturing techniques, and the ones produced by the food industry. Their physical and chemical properties, benefits, and drawbacks were described, as well as the studies that examined their employment as building products. As this collection of studies demonstrated, many possibilities have already been investigated, considering several materials and types of composites. For example, Azevedo et al. (de Azevedo et al., 2022) evaluated different agro-industrial solid wastes (pineapple, sugar cane, açaí, coconut, and rice) to produce cementitious materials, such as mortars and concretes; Solt et al. (Solt et al., 2019) analysed formaldehyde-free adhesives for particleboards' production and

Nomenclature

A	Samples area [m^2].	σ	Stress [N/mm^2].
ρ	Apparent density [kg/m^3].	ε	Strain [-].
α	Sound absorption coefficient.	F	Applied force [N].
R	Airflow resistance [Pa.s/m^3].	l	Sample span [mm].
Δp	Air pressure difference [Pa].	b	Sample width [mm].
qv	Air flow rate [m^3/s].	h	Sample thickness [mm].
r	Airflow resistivity [kPa.s/m^2].	δ	Displacement [mm].
d	Thickness [m] (in air flow resistivity eq.).	$δ_{max}$	Maximum displacement [mm].
m_0	Initial mass [kg].	E	Modulus of elasticity [N/mm^2].
$m_{d(n-1)}$	Mass of previous desorption cycle [kg].	$σ_{60\%}$	σ at 60% of F_{max} [N/mm^2].
m_{an}	Mass of considered absorption cycle [kg].	$σ_{20\%}$	σ at 20% of F_{max} [N/mm^2].
m_{dn}	Mass of considered desorption cycle [kg].	$ε_{60\%}$	ε at 60% of F_{max} [-].
$ρ_{A,ac}$	Moisture sorption [kg/m^2].	$ε_{20\%}$	ε at 20% of F_{max} [-].
$ρ_{A,dc}$	Moisture desorption [kg/m^2].	Δσ	Difference between $σ_{60\%}$ and $σ_{20\%}$ [N/mm^2].
$ρ_{A,sc}$	Moisture content difference [kg/m^2].	Δε	Difference between $ε_{60\%}$ and $ε_{20\%}$ [-].
MBV	Moisture buffering value [g/(m^2.% RH)].	A_0	Sample initial cross-sectional area [mm^2].
MBV_a	MBV during the sorption phases [g/(m^2.% RH)].	d_0	Sample initial thickness [mm].
MBV_d	MBV during the desorption phases [g/(m^2.% RH)].	f_0	Normal incidence sound absorption.
RH	Relative humidity [%].	k	Apparent dynamic longitudinal elastic modulus.
RH_{high}	Highest value of RH (considered 75%) [%].	M_{eff}	Effective mass [kg].
RH_{low}	Lowest value of RH (considered 50%) [%].	F_{10}	Force at 10% strain [N].
$σ_{max}$	Flexural strength [N/mm^2].	$δ_{10}$	Displacement at 10% strain [mm].
F_{max}	Maximum applied force [N].	$σ_{10}$	Compressive strength at 10% strain [N/mm^2].
		E_{10}	Modulus of elasticity [N/mm^2].

reported cashew nut shell liquid; Rault et al. (Raut et al., 2011) and Muñoz Velasco et al. (Muñoz Velasco et al., 2016) considered bricks' production by using cotton waste and coffee grounds, respectively.

Among the several types of building composites, particleboards were widely investigated. They seemed to be promising building products for their versatility (e.g., employed in floors, ceilings, divider walls, and furniture), their affordability, and their sustainability (Gürü et al., 2015; Mahieu et al., 2019; Rubino et al., 2023). Furthermore, they ensured easy use of different types of bio-wastes, such as banana tree fibres (Nunes et al., 2017), hemp (Auriga et al., 2022; Pennacchio et al., 2017), corn cob (Ramos et al., 2021), flax fibres (Sam-Brew and Smith, 2015) and tree bark (Tudor et al., 2021).

In addition to these, some of the main addressed topics in modern research are the use of materials not harmful to human health and the improvement of indoor air quality and comfort (Fratoni et al., 2019), which can lower operational costs too (Posani et al., 2022, 2021). Therefore, one of the biggest challenges is the proposal of eco-friendly materials, able to passively ensure good indoor conditions, guaranteeing the well-being of both the environment and the users, and lowering energy requirements.

Two types of indoor comfort could be considered: hygrothermal and acoustic. The hygrothermal comfort is related to the operative temperature, a combination of air temperature and mean radiant temperature in the room (Posani et al., 2023). It depends on several factors, sometimes difficult to forecast (Ranesi et al., 2022). Therefore, a simplified evaluation was usually considered, involving information such as the predicted mean vote (PMV), predicted percentage of dissatisfaction (PPD), internal temperature, and relative humidity. The acoustic comfort is related to the protection against noise and is mainly guaranteed by adequate sound insulation (Sakthivel et al., 2021). Moreover, the control of the indoor acoustic environment is a crucial factor that enhances the comfort and well-being of the users (D'Orazio et al., 2020; De Salvio et al., 2023). This purpose makes a proper distribution of the materials necessary, as their acoustic performance may depend on their layout (Fratoni et al., 2023), relative humidity, and temperature (Cingolani et al., 2022).

Bio-based building materials seemed to be an efficient possibility for both types of comfort. Hence, apart from the low environmental impact and eco-friendly aspects, bio-wastes showed several benefits when incorporated into building products, namely sound absorption capacity (Martellotta et al., 2018; Othmani et al., 2017), thermal insulation performance (Muizniece and Blumberga, 2016; Platt et al., 2023), passive control of the hygrothermal indoor conditions and the air quality (Liuzzi et al., 2018), as well as mechanical resistance (Molari et al., 2017; Nadhari et al., 2019) to enable applicability. Past research already demonstrated that bio-wastes could have promising thermal insulation and acoustic absorption performance. Hence, they could improve hygrothermal and/or acoustic indoor comfort. For example, Trobiani Di Canto et al. (Trobiani Di Canto et al., 2023) employed wheat bran and the waste material banana peel to produce a thermal insulation board. Ricciardi et al. (Ricciardi et al., 2021) considered cork scraps, rice husk, and coffee chaff as bio-wastes and reported their promising thermal insulation performance. Martellotta et al. (Martellotta et al., 2018) demonstrated that wastes deriving from olive pruning could produce a composite with interesting acoustic behaviour. Tang et al. (Tang et al., 2018) evaluated the acoustic properties of corn husk and concluded that it had good acoustic absorption performance, appropriate for noise reduction.

However, bio-waste-based building composites also have some drawbacks, such as high hygroscopicity and low resistance to water and fire (Bakatovich et al., 2022), which can cause their degradation. Moreover, the presence of nutrients and the organic composition may increase the susceptibility to biological attack, a severe hazard both for materials and users (Ginestet et al., 2020) since it can lower composites' performance, degrade indoor air quality, and cause human diseases (Echeverria et al., 2021; Stefanowski et al., 2017). This drawback can be moderated or prevented by adding additives, physical or chemical treatments, the employment of specific strategies, and constant monitoring (Chastre et al., 2023; de Carvalho et al., 2020; Dennis et al., 2021).

Starting from this knowledge, the present work investigates the feasibility of producing a bio-based composite (i.e., bio-based board), for

internal use that could improve indoor comfort (hygrothermal and/or acoustic). Unconventional materials not harmful to human health were selected, considering both the benefits and drawbacks of bio-based composites (Cintura et al., 2023a). The bio-resource guaranteed the bio-based aspect. Among the many benefits, the selected adhesive moderated some of the bio-based products' weaknesses.

Arundo donax L. (commonly known as giant reed or giant cane) is an herbaceous, perennial, and non-food crop, native to Asia but invasive in many regions of the world. It consists of stems 4 – 6 m high, diameters between 2 and 3 cm, and 2 – 3 mm thick. Due to its high tolerance to different climates and soil conditions, it can be found worldwide, mainly in southern Europe (Caponetto et al., 2023; Jámbor and Török, 2019; Molari et al., 2021). The annual crop yield depends on several factors, such as the soil, climate, use of fertilisation, and irrigation. Hence, past studies that quantified this information reported different results. Ceotto et al. (Ceotto et al., 2021) carried out a three-year experiment and achieved an annual dry matter yield of up to 51.4 Mg DM ha^{-1} (higher in the case of a harvesting treatment). Furthermore, the researchers reported a medium-term (6 years) and a long-term experiment (12 years) that achieved a dry matter yield of about 39.6 Mg ha^{-1} and 37.7 Mg ha^{-1}, respectively. Alexopoulou et al. (Alexopoulou et al., 2015) evaluated *A. donax*'s long-term productivity (11–22 years) in the Mediterranean South area. The researchers achieved a mean annual biomass production of 15.7 Mg DM ha^{-1} of *A. donax*. Considering long-term production, a value of 13.6 Mg DM ha^{-1} year^{-1}. Danelli et al. (Danelli et al., 2021) reported that past research achieved yields of up to 20 Mg DM ha^{-1}.

Its wide availability and properties made *A. donax* employed for several purposes, such as producing musical instruments for the paper industry, as a source of biomass, biofuel, and building practices (Malheiro et al., 2021). As for this latter, it was already employed for panels, reinforcement for concrete and plasters, support for roofs and coverings, or in ceilings. It contributed to thermal insulation and promising mechanical performance (Barreca, 2012; Malheiro et al., 2021). Molari et al. (Molari et al., 2021) provided a mechanical characterization of *A. donax*. They demonstrated that it could be employed as a structural material, although it has not commonly been used as such. Carneiro et al. (Carneiro et al., 2016) developed and characterized a new construction technology, based on the cob earth technology by turning it lightweight (known as *ReedCob*) by using mainly *A. donax* and earth. The researchers demonstrated the feasibility of using this construction system. They reported its several benefits: low density and high thermal insulation performance, high mechanical flexural strength, and easy and fast production. Fiore et al. (Fiore et al., 2014) analysed the properties of *A. donax* and concluded that it could be used as reinforcement in polymer composites. García-Ortuño et al. (García-Ortuño et al., 2011) demonstrated the feasibility of producing particleboards by using shredded *A. donax* particles as aggregates and urea formaldehyde resin as adhesive.

As the knowledge of the physical and chemical properties of raw materials could help to understand the performance of the final composites better (Cintura et al., 2021; Viel et al., 2018), some properties of *A. donax* available from previous studies (Fiore et al., 2014; Molari et al., 2021) are reported in Table 1. The differences between the values are expected to be derived from the employed test methods and conditions (e.g., regions of growing, test setup, sizes of samples, laboratory conditions, and samples' moisture content).

Considering the benefits of using giant reed and its promising performance, in the present work, it was employed as the aggregate (by shredding the stems in particles), though in the past it has been studied mainly as fibres. Indeed, according to past research related to bio-based composite, the employment of bio-wastes and bio-resources as particles/high-mass aggregates is not so commonly investigated (Faruk et al., 2012; Sanjay et al., 2018; Savio et al., 2022).

As for the adhesive, a sodium silicate solution was considered due to its several benefits, such as its bonding capacity and its non-toxic nature (Lee and Thole, 2018; Liuzzi et al., 2020a). Indeed, in addition to the

Table 1

Physical and chemical properties of A. donax reported in past studies (Fiore et al., 2014; García-Ortuño et al., 2011; Malheiro et al., 2021; Molari et al., 2021).

Property	Values	References
Real density [kg/m^3]	1168 ± 3	(Fiore et al., 2014)
Bulk density [kg/m^3]	893	(Fiore et al., 2014)
Apparent density (C-shape) [kg/m^3]	577	(Molari et al., 2021)
	476–524	(Malheiro et al., 2021)
	583	(Malheiro et al., 2021)
Cellulose content [%]	43.59	(Fiore et al., 2014)
Hemicellulose content [%]	20.5	(Fiore et al., 2014)
	28.48–32.03[a]	(García-Ortuño et al., 2011)
Lignin content [%]	17.2	(Fiore et al., 2014)
	17.70–21.31[a]	(García-Ortuño et al., 2011)
Ash [%]	1.9	(Fiore et al., 2014)
	3.00–6.14[a]	(García-Ortuño et al., 2011)
Thermal conductivity [W/(m.K)]	0.06	(Bakatovich et al., 2022)
Tensile strength [N/mm^2]	248	(Fiore et al., 2014)
	103.7–127.4[b]	(Molari et al., 2021)
Young's modulus - Tension [N/mm^2]	15.3	(Molari et al., 2021)
Compressive strength [N/mm^2]	57	(Molari et al., 2021)
Young's modulus - Compression [N/mm^2]	13.4	(Molari et al., 2021)

Note: [a] The lowest and highest values are reported (without differentiating node and internode); [b] Values for samples with node and internode, respectively.

sustainability and eco-efficient aspects, the non-harmfulness of the final composites must be guaranteed. This could be provided by avoiding dangerous products, such as formaldehyde-based adhesives which can be hazardous to human health (Lee et al., 2020; Owodunni et al., 2020). Furthermore, the sodium silicate solution may improve the resistance to biological attack and chemical decomposition (Lee and Thole, 2018; Liuzzi et al., 2020a), which can shorten the service life of building materials (Jones et al., 2022). Finally, as reported before, the sodium silicate solution was selected to avoid high pressure in the production process and high temperatures for drying and curing to secure lower environmental impact (Cintura et al., 2023a). Nevertheless, some drawbacks were reported: the sodium silicate solution employed as an adhesive demonstrated high hygroscopicity and low bonding strength in wood-based composites (Lee and Thole, 2018; Song et al., 2021).

The production process and the experimental campaign were described in a previous study (Cintura et al., 2023c) characterizing a hazelnut shell-sodium silicate solution composite. This enabled the comparison between different bio-wastes/bio-resources employed as aggregates with the sodium silicate solution as the adhesive. As Bakatovich et al. (Bakatovich et al., 2022) investigated a similar giant reed-based composite but with some differences in the binder and different aggregate grain sizes, this work was considered to compare the results.

Hygrothermal, acoustic, and mechanical properties were evaluated to provide a general characterization of the produced boards, and this contributed to defining the most promising applications. The work aimed at demonstrating the feasibility of producing a bio-based board for indoor application to both lowering the environmental impact and improve indoor comfort. Furthermore, it intended to describe a methodology for a wide-range analysis of unconventional building composites, which could be useful for future research.

2. Materials and methods

2.1. Materials

2.1.1. Giant reed

Giant reed was collected from a cultivation of the Department of Agricultural and Food Sciences, of the University of Bologna, in Cadriano, Bologna, Italy. It was harvested and air-dried in the

Laboratory at room temperature for one year. The reeds were cut to have grain sizes mainly between 4 mm and 8 mm to secure the feasibility of producing boards (Cintura et al., 2023b), and using aggregates with similar particle size distribution as the reference study (Cintura et al., 2023c), even if differing for the elongated shape. Giant reed was then dried at T = 60 °C until constant mass (variation in mass less than 0.1% after 24 h) and characterized according to the recommendation of the RILEM Technical Committee 236-BBM "Bio-aggregate-based building materials" (Amziane et al., 2017). The initial water content was (6.43 ± 0.08) %, and the loose bulk density was (181.3 ± 6.3) kg/m³ . Fig. 1 shows the particle size distribution and the employed giant reed. Other properties of *A. donax* have been previously reported in the literature (Table 1).

2.1.2. Sodium silicate solution

As for the adhesive, a sodium silicate solution, $Na_2O \bullet n(SiO_2)$, provided by Ingessil Srl, Montorio (VR), Italy, was employed coherently with the previously described aims, hence considering the reference study (Cintura et al., 2023c). Table 2 summarizes its properties.

2.2. Samples preparation

The mix design and the production process were selected considering the reference past studies (Cintura et al., 2023b, 2023c), that evaluated the feasibility of producing composite boards made of hazelnut shells as high-mass bio-aggregates and sodium silicate solution as the adhesive. The mix design and the production process were defined after several practical tests to obtain the most sustainable building composite, maximizing the use of hazelnut shells, minimizing the amount of sodium silicate solution, and guaranteeing samples' production. Indeed, fewer quantities of adhesive did not allow sufficient mechanical resistance. Both the production process and the materials' quantities were kept the same for easier comparison between the results, as previously reported, ensuring that the type of bio-aggregates was the only different parameter. Hence, the percentages (by volume) of giant reed and sodium silicate solution were 70–30%, respectively.

The aggregates and the adhesive were mechanically mixed for 10 min until homogeneity (Fig. 2a) and then placed into silicon or wooden moulds (thickness = 4 cm), without being compacted, and levelled by using a spatula (Figs. 2b and 2c) to have a horizontal surface. The 4 cm thickness was selected as it was suitable for both thermal and acoustic boards. Furthermore, it was a good compromise for the feasibility of production and the implementation of the tests, and its

Table 2
Properties of the employed sodium silicate solution provided by Ingessil Srl (Ingessil).

Property	Value
Weight ratio [-]	2.40
Density [°Bè]	46.45
Molar ratio [-]	2.48
Sodium silicate concentration [% p/p]	41.33
SiO_2 [% p/p]	29.17
Na_2O [% p/p]	12.16
Density [g/ml] at T = 20 °C	1.471
pH [-] at T = 20 °C	12.40

representativeness, considering the size of the bio-aggregates used. Lower thickness could also determine problems related to samples' resistance, while a higher one could determine composites too heavy to be easily analysed. The moulds were closed by fixing a wooden top (Fig. 2d) and put at T = 60 °C for 3 h, then air-dried, constantly rotated every 30 min (for half a day) to secure a homogeneous distribution of the sodium silicate solution. After 2 days, the samples were demoulded, cured at laboratory conditions for 28 days, and dried at T = 50 °C until reaching a constant mass (considered as a variation in mass in 24 h less than 0.5%) to secure a complete drying (Liuzzi et al., 2020a, 2020b).

Fig. 2e shows some rectangular and cylindrical composite samples (10 cm x 10 cm x 4 cm, and diameter = 10 cm and high = 4 cm, respectively).

2.3. Test methods

All tests were performed after drying the samples at T = 50 °C until reaching a constant mass (variation in mass in 24 h less than 0.5%), as previously described (Section 2.2). The evaluated properties, the number, designation, and sizes of the produced composite samples, and the relevant references are summarized in Table 3. Further details are described in the following sections.

2.3.1. Visual observation and qualitative evaluation of the production process

The slow absorption of the sodium silicate solution by the aggregates could result in non-perfectly uniform samples, required for a correct evaluation of the properties of the composite. The samples were constantly monitored during drying and curing time to avoid this drawback. The visual analysis provided a qualitative evaluation of the
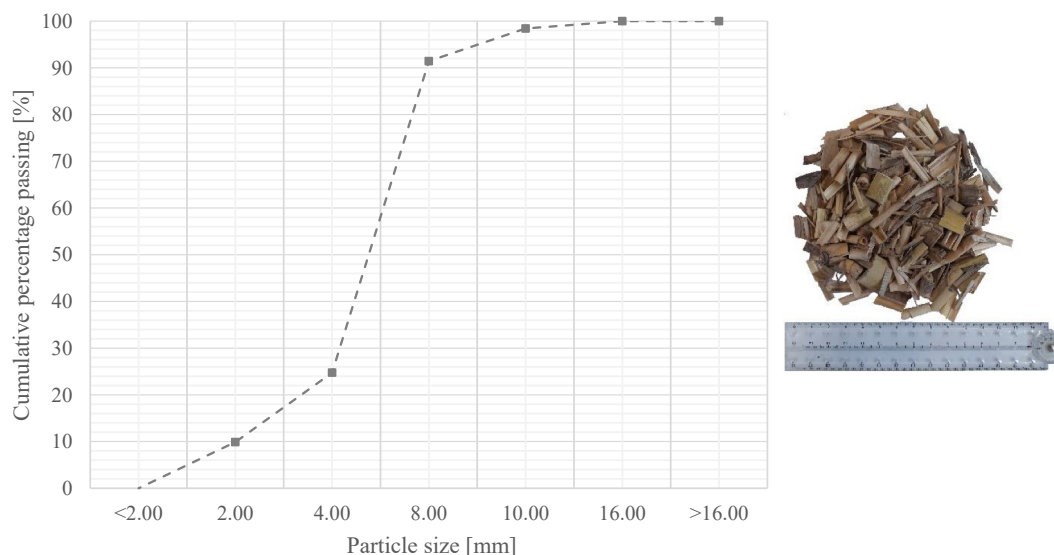

Fig. 1. Particle size distribution and the employed giant reed.

Fig. 2. Some steps of the production process of composite samples made of giant reed and the sodium silicate solution: a) mechanical mixing of the aggregates and the adhesive; b) moulding (wooden mould 50 cm × 50 cm × 4 cm) by using a spatula; c) cylindrical mould (diameter = 10 cm, high = 4 cm) with the mixture of giant reed and sodium silicate solution; d) closed moulds (10 cm × 10 cm × 4 cm); e) rectangular and cylindrical composite samples after demoulding and curing phase.

Table 3
Tests performed, number, designation, and dimensions of composite samples, and considered references.

Properties	Composite samples			References
	Number	Designation	Sizes [cm] (high = 4 cm)	
Visual observation	All	-	Varied	(Cintura et al., 2023b)
Apparent density	6	A1, A2, A3, A4, A5, A6	10 x 10	(EN 323:1993)
Thermal conductivity	2	A10, A11	50 x 50	(EN 12667:2001)
Hygroscopicity	6	A1, A2, A3, A4, A5, A6	10 x 10	(ISO 24353:2008)
Sound absorption	3	A7, A8, A9	Diameter = 10	(ISO 10534-2:2001)
Air flow resistivity		A7, A8, A9	Diameter = 10	(ISO, 9053–2:, 2020, 2020)
Flexural strength	6	A10_01, A10_02, A10_03, A11_01, A11_02, A11_03	50 x 10 (cut)	(UNI 11842:2021)(ISO 14125:1998 +A1:2011)
Compressive strength	10	A10_01_A, A10_01_B, A10_02_A, A10_02_B, A10_03_A, A11_01_A, A11_01_B, A11_02_A, A11_02_B, A11_03_A	10 x 10 (cut)	(EN 826:2013)

correctness of the production process. Furthermore, qualitative considerations by visual checks after each test were made.

2.3.2. Apparent density and thermal conductivity

The apparent density was measured by adapting EN 323 (EN 323:1993), hence by weighting three samples (stabilized at T = 50 °C) by an electronic balance Kern EW 2200–2NM, by determining their dimensions by a Fervi Digital Caliber, and finally by calculating the ratio between mass and volume (Fig. 3a) and considering the average value and standard deviation as the representative value.

The thermal performance can be evaluated through different methods, classified as steady state and transient methods (Posani et al., 2022). The steady-state methods analyse the thermal performance in equilibrium conditions, hence when temperature throughout the sample remains constant. Although the steady-state technique requires larger samples, more expensive equipment, and more time than the transient method, it was selected to provide the most accurate results (Yüksel, 2016). Hence, thermal conductivity was determined by the heat flow method, according to EN 12667 (EN 12667:2001).

The samples 50 cm × 50 cm × 4 cm were stabilized at T = (20 ± 1) °C and RH = (60 ± 5) % and placed between two different plates (heated and cooled). Thermal conductivity was assessed by measuring the heat flow through the samples, namely the capacity of conducting heat, using the equipment described and validated by Baldinelli et al. (Baldinelli et al., 2019), and reported in Fig. 3b. The samples' mass was evaluated before and after the test to ensure that moisture content remained constant, as this parameter could affect the final results (Liuzzi et al., 2017; Palumbo et al., 2016). The average values and the standard deviation of the thermal conductivity were considered.

2.3.3. Hygroscopicity properties

The hygroscopicity of the composite was evaluated according to ISO 24353 (ISO 24353:2008). The laboratory test consists of subjecting the samples to different relative humidity levels, by measuring the variation in mass over time and determining the moisture sorption/desorption capacity. A moisture barrier, consisting of an adhesive aluminium foil that enabled the sealing, was applied all over the samples, except for a single surface corresponding to the top of the samples (A = 0.1 m^2).

Fig. 3. Main tests of the experimental campaign: a) evaluation of the apparent density of a giant reed-based composite sample; b) equipment to evaluate the thermal conductivity by the heat flow method; c) composite samples into the climate chamber during the hygroscopicity test; d) a cylindrical sample of giant reed into the impedance tube to evaluate the sound absorption capacity; e) giant reed-based sample (10 cm x 50 cm x 4 cm) in the Galdabini machine at the beginning of the bending test; f) giant reed-based sample (10 cm x 10 cm x 4 cm) before the performance of the compressive test.

First, they were placed in a climate chamber (Climatest ARGOLab CH 250), preconditioned at T = (23 ± 1) °C and RH = (63 ± 5) % until reaching a constant mass (change in mass of less than or equal to 0.5% over 24 h) and weighed ($m_0 = m_{d(n-1)}$). Then, the samples were conditioned at T = (23 ± 2) °C, RH = (75 ± 2) % for 12 h (sorption phase) and weighed every 3 h (m_{an}), and at T = (23 ± 2) °C, RH = (50 ± 2) % for 12 h (desorption phase) and weighed (m_{dn}) (Fig. 3c), as required by ISO 24353 (ISO 24353:2008). This procedure was repeated four times (four cycles). Moisture sorption ($\rho_{A,ac}$) and desorption ($\rho_{A,dc}$) content, and moisture content difference ($\rho_{A,sc}$) were determined according to Eqs. 1, 2, and 3, respectively.

$$\rho_{A,ac} \quad \left[\frac{kg}{m^2}\right] = \frac{m_{an} - m_{d(n-1)}}{A} \tag{1}$$

$$\rho_{A,dc} \quad \left[\frac{kg}{m^2}\right] = \frac{m_{an} - m_{dn}}{A} \tag{2}$$

$$\rho_{A,sc} \quad \left[\frac{kg}{m^2}\right] = \rho_{A,ac} - \rho_{A,dc} \tag{3}$$

The moisture buffering value (MBV), which quantifies the amount of absorbed and released moisture considering cycling between two levels of RH (Ansell et al., 2020), was evaluated by adapting and simplifying the method defined by Rode et al. (Rode et al., 2005), as the average value between MBV during the sorption phase (MBV_a), described by Eq. 4 and for the desorption (MBV_d), calculated as reported in Eq. 5. The values of the last three cycles were considered.

$$MBV_a \left[\frac{g}{m^2\%RH}\right] = \frac{m_{an} - m_{d(n-1)}}{A} \frac{1}{x(RH_{high} - RH_{low})} \tag{4}$$

$$MBV_d \left[\frac{g}{m^2\%RH}\right] = \frac{m_{an} - m_{dn}}{A} \frac{1}{x(RH_{high} - RH_{low})} \tag{5}$$

where RH_{high} is the highest value of RH (75%) and RH_{low} is the lowest one (50%). Although the conditions were different from the reference (Rode et al., 2005), namely different values of RH and different durations of the sorption/desorption cycles, the result provided a quantitative value to describe the moisture buffering capacity of the analysed composites and enabled a comparison with past studies.

2.3.4. Acoustic properties

The sound absorption capacity can be evaluated by several techniques, divided into empirical models and inverse methods – i.e., considering physical properties strictly related to acoustic absorption, such as air flow resistivity, flexural and compressive strength – and direct measurements using an impedance tube (Othmani et al., 2017; Rey et al., 2012). This latter method is standardized and described by ISO 10534–2 (ISO 10534–2:2001): a sample is placed at the end of a tube (Kundt's tube), where an acoustic excitation is generated, and acoustics pressure is registered by microphones. The value of the incidence absorption coefficient is determined by measuring the sound wave variations and using some corrective formulas. Although the direct measurement method provides only the normal incidence sound absorption and could be subjected to errors due to the placement of the samples in the tube (Martellotta et al., 2018), it was selected for its several advantages, such as the rapid evaluation, the possibility of using small samples and the easy test implementation (Rubino et al., 2023).

Three conditioned samples (diameter =10 cm, high = 4 cm) at T = (20 ± 1) °C and RH = (60 ± 5) %, were smoothed, placed at the end of a Plexiglas Kundt's tube, and sealed with plasticine to reduce the possible gaps between them and the tube (Fig. 3d). An exponential sine sweep (Corredor-Bedoya et al., 2021) was generated by a loudspeaker and a signal amplifier (Samson 120 A with SNR = 96 dB) and converted to an analogue signal by the Digital to Analog Converters of the soundcard (RME 802). The signal was recorded by a single microphone 1/2" PCB and converted by the Analog-to-Digital Converter (sample rate of

44.1 kHz at 24-bit depth), and processed by ITA-Toolbox (Berzborn et al., 2017) through the Transfer-Function Method (Chung and Blaser, 1980a, 1980b). The test was performed for each sample's front and back sides to avoid possible measurement errors caused by producing non-perfectly uniform samples.

2.3.5. Air flow resistivity

The measurement of airflow resistance of porous and fibrous acoustical materials was standardised in ISO 9053–2 (ISO 9053–2:2020) and ASTM C-522-03 (ASTM C522–03:2022), which described the measurement equipment and the test procedure. The airflow resistance of a material is defined by Eq. 6 as:

$$R\left[\frac{Pa \times s}{m^3}\right] = \frac{\Delta p}{q_v} \tag{6}$$

where Δp [Pa] is the air pressure difference across the sample with respect to the atmosphere and q_v [m^3 /s] the air flow rate through the sample. One derived quantity of great interest in applied acoustic is the airflow resistivity, *r*, defined by Eq. 7 as:

$$r\left[\frac{Pa \times s}{m^2}\right] = \frac{\Delta p}{q_v} \times \frac{A}{d} \tag{7}$$

where A [m^2] is the section of the tested sample and d [m] is the thickness of the tested sample (considered homogeneous) in the flow direction. In the latest version of ISO 9053–2 (ISO 9053–2:2020), σ was used to identify airflow resistivity. Still, in this article, σ denotes "Stress"; so the old notation *r* used in ISO 9053:1991 was considered to avoid misunderstanding.

The measurements of airflow resistivity were carried out on each sample three times by using the equipment described by Schiavi et al. (Schiavi et al., 2011). The same samples employed to evaluate the sound absorption capacity (diameter = 10 cm, high = 4 cm) were considered. Each sample was placed with the rougher side facing the environment and the flatter side facing the inside of the measurement tube.

2.3.6. Flexural strength

The flexural properties were evaluated using a four-point bending test, adapting UNI 11842 (UNI 11842:2021) and ISO 14125 (ISO 14125:1998 +A1:2011). The samples used in the thermal analysis (A10 and A11) were cut into strips 10 cm x 50 cm x 4 cm. The designations, namely A10_01, A10_02, A10_03, A11_01, A11_02, A11_03, highlighted the considered original sample.

The six samples were conditioned at T = (20 ± 1) °C and RH = (60 ± 5) %, and tested at laboratory conditions in displacement control by using a Galdabini universal machine (maximum capacity of 100 kN) with a velocity of 0.5 mm/min. The supports' distance was 39 cm. Hence, the force was applied each 13 cm, as shown in Fig. 3e. Some samples were placed with the rougher side as the lower one (samples ROU_LOW) and the others in the opposite way, namely with the rougher side as the upper one (samples ROU_UP) to evaluate the bending performance for both faces. A linear displacement transducer, LVDT, HBM Model WA20mm, recorded the force and displacement during the test to determine the stress-strain curve defined by Eqs. 8 and 9, and the flexural strength σ_{max} [N/mm^2] of each sample calculated as the one corresponding to the maximum applied force, F_{max} [N] (Eq. 10).

$$\sigma_{(intrados)}\left[\frac{N}{mm^2}\right] = \frac{Fl}{bh^2} \tag{8}$$

$$\varepsilon_{(intrados)}\left[-\right] = \frac{108}{23}\frac{h\delta}{l^2} \tag{9}$$

$$\sigma_{(max)}\left[\frac{N}{mm^2}\right] = \frac{F_{max}l}{bh^2} \tag{10}$$

where F [N] is the applied force, l [mm] is the span of the sample, b [mm] and h [mm] are the width and thickness of the sample, respectively, and δ [mm] is the displacement. The test was carried out until reaching the breaking load, or the maximum displacement that the LVDT could register. The measurements were carried out for each sample; therefore, the average values and standard deviation were considered. The modulus of elasticity, E, was calculated as described in Eq. 11, by considering the values of σ and ε at 20% and 60% of the maximum applied load, F_{max}, (UNI 11842:2021):

$$E\left[\frac{N}{m^2}\right] = \frac{\Delta\sigma}{\Delta\varepsilon} = \frac{\sigma_{60\%} - \sigma_{20\%}}{\varepsilon_{60\%} - \varepsilon_{20\%}} \tag{11}$$

2.3.7. Compressive strength

Compressive behaviour was determined by adapting EN 826 (EN 826:2013). The undamaged extremities of the strips used for the bending test were cut to produce samples 10 cm × 10 cm × 4 cm, as reported in Table 3. The designation highlighted the original sample, which was employed first for thermal analysis, and then for bending test. The rectangular samples were placed between the two plates in the Galdabini machine (maximum capacity of 100 kN), with a joint of 11.65 kg, and compressed at a velocity of 2 mm/min (Fig. 3f).

Eqs. 12 and 13 describe the relation to determine the stress-strain curve, considering F [N] as the applied force and δ [mm] the displacement during the test, both recorded by the LVDT (HBM Model WA20mm), A_0 [mm^2] the initial cross-sectional area of the samples, and d_0 [mm] the initial thickness of the samples.

$$\sigma\left[\frac{N}{m^2}\right] = \frac{F}{A_0} \tag{12}$$

$$\varepsilon[-] = \frac{\delta}{d_0} \tag{13}$$

Compressive strength was determined by considering the average and standard deviation of the compressive stress corresponding to the breaking load or 10% strain (thus, $\varepsilon = 0.1$ if the samples did not achieve rupture), as defined by EN 826 (EN 826:2013). The modulus of elasticity was determined by Eq. 11, considering the σ and ε at 20% and 60% of the compressive strength.

3. Results

3.1. Visual observation and qualitative evaluation of the production process

All the samples seemed sufficiently uniform at the end of the curing time. However, some seemed to have a higher amount of sodium silicate on one side (the base of the samples). As this possible problem had been foreseen, more than the minimum recommended number of composite samples were produced and tested (e.g., for the apparent density and the hygroscopicity test six samples were considered) and laboratory tests were performed for both sides of the samples whenever necessary, as described in Section 2.3.

No biological colonization was visually observed, neither after the hygroscopicity tests, namely after placing the samples at RH = 75% for 12 h, four times.

3.2. Apparent density and thermal conductivity

Table 4 reports the apparent density values at T = 50 °C, thermal conductivity at T = 20 °C, and RH = 60%, the average values for both, and the standard deviation (S.D.) for the apparent density.

The variations among the samples could have occurred due to the production process, namely due to the uncontrolled distribution of different grain sizes aggregates, and the sodium silicate solution. The samples could have some differences in aggregate sizes, internal

Table 4
Results of apparent density at T = 50 °C, thermal conductivity at T = 20 °C, RH = 60% for each tested composite sample, average value, and standard deviation (S.D.).

Composite samples	Apparent density [kg/m^3]	Thermal conductivity [W/ (m. K)]
A1	434	-
A2	518	-
A3	642	-
A4	493	-
A5	518	-
A6	499	-
A10	-	0.123
A11	-	0.132
Average ± S.D.	517 ± 68	0.128

porosity, and voids' volume. All these possibilities were reported by the standard deviation, which was low if related to the average value. Hence, a good uniformity between the tested samples was guaranteed.

The mass variation of the samples employed to evaluate the thermal performance (weighed before and after the test) was less than 0.5%. The moisture content was considered constant.

3.3. Hygroscopicity and Moisture Buffering Value

Fig. 4 shows the moisture content along the time for the four adsorption/desorption cycles.

The composite demonstrated high hygroscopicity, with moisture sorption content greater than moisture desorption for all cycles, being $\rho_{(A,ac)} = 0.13$ kg/m^2 and $\rho_{(A,dc)} = 0.08$ kg/m^2 at the beginning of the test, and $\rho_{(A,ac)} = 0.14$ kg/m^2 and $\rho_{(A,dc)} = 0.08$ kg/m^2 after the four cycles (average values of the composite samples). The moisture content difference was almost the same for all cycles, between 0.04 kg/m^2 and 0.07 kg/m^2 (average values). The differences between the samples might derive from a different distribution of the sodium silicate solution in the exposed surface, which could determine different moisture absorption capacities. The moisture storage capacity was more significant than the release one during the test; the composite samples were so hygroscopic that they did not stabilise after each of the four cycles.
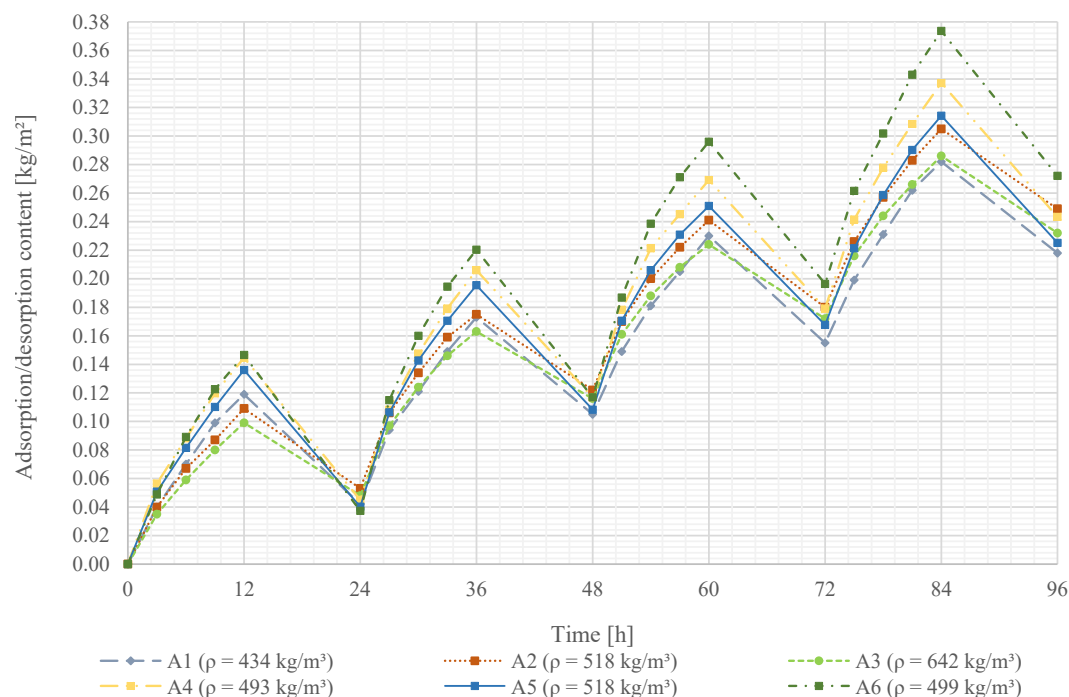
As described in Section 2.3, the MBV was calculated and rated considering the Nordtest methodology (Rode et al., 2005), even if this defined the practical MBV by considering different conditions: 8 h-sorption phase and 16 h-desorption phase at RH = 75% and RH = 33%, respectively. In the present work, the MBV was calculated according to the sorption/desorption phases' conditions described in ISO 24353 (ISO 24353:2008). This could determine some differences in the results. Hence, this information should be considered for comparisons and discussions. The MBV was (4.33 ± 1.84) g/(m^2 %RH) (average value of the six tested samples) and the giant reed-based composite can be rated as "Excellent" (MBV > 2).

3.4. Acoustic properties

Fig. 5 reports the results of the acoustic absorption coefficient evaluated for both sides of the samples: the dotted lines represent the results for the rougher ones (samples A). In contrast, the continuous lines represent the results for the flatter sides (samples B).

The acoustic absorption behaviour was the same for all samples with differences in the absorbed frequencies, especially for two of them, which had the exposed sides as the flatter ones and absorbed higher frequencies (almost 1100 Hz). The variations could be caused by the differences in the disposition of the aggregates, hence the distributions of internal voids. Indeed, as de Carvalho et al. (de Carvalho et al., 2020) reported, aggregates' particle sizes and distribution could widely influence the results. At frequencies between 600 Hz and 700 Hz, the sound absorption coefficient, α, was almost 1; the curve reached a peak, decreased, and then slightly increased again.

The most common acoustic absorption behaviours are due to porous materials, membrane absorbers, and resonators. Porous materials are widely used for their great acoustic performance (Koizumi et al., 2002), provided by the porosity: when a sound wave strikes the material's surface, it causes the vibration of the internal air molecules transforming the sound into energy (viscous and dissipation phenomena). Porous absorbers usually work at high frequencies and their performance varies depending on the thickness (Selvaraj et al., 2019). Due to the resonance phenomenon, the membrane absorbers and resonant absorbers can absorb lower frequencies. At specific frequencies, the absorbers can
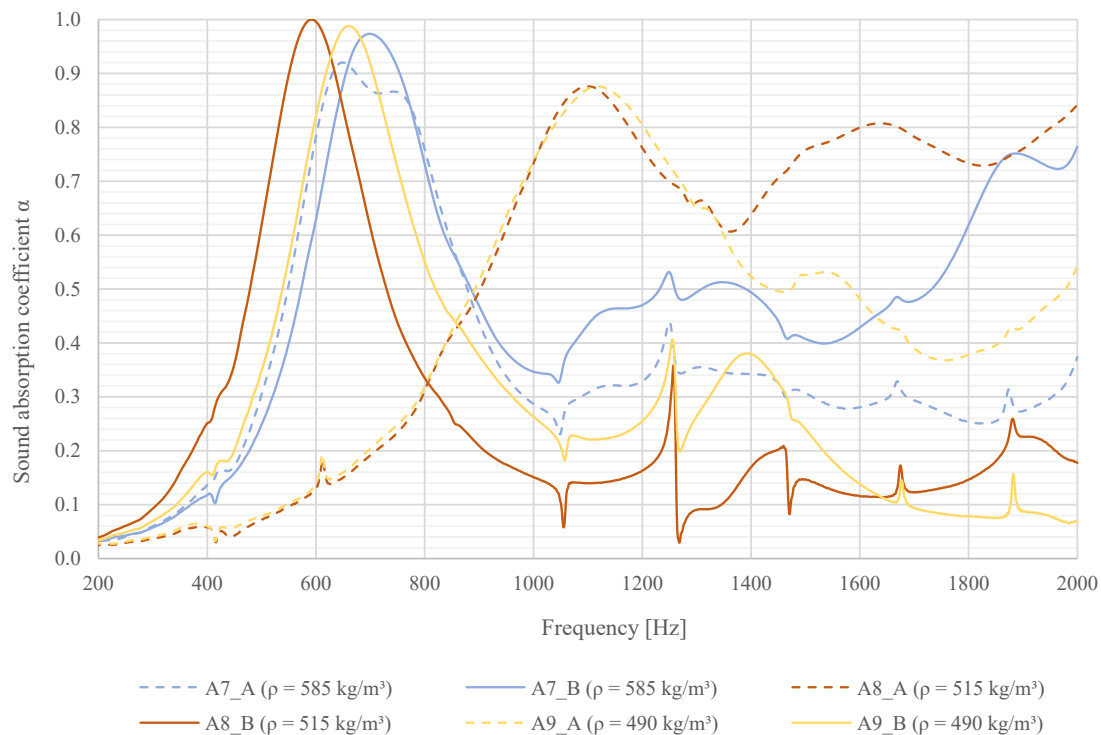

Fig. 4. Moisture adsorption/desorption for four cycles of the tested composite samples.

Fig. 5. Sound absorption coefficients of both sides of the three tested samples. Continuous lines represent the flatter exposed surfaces' results and the rougher ones' dotted lines.

freely vibrate (membrane absorbers) or the interaction between the sound wave and the air molecules inside the voids acts as a spring-mass system (resonant absorbers). In this latter case, the vibration enabled the dissipation of the acoustic wave, even in more complex configurations (Cingolani et al., 2021).

The giant reed-based composite showed a less common acoustic-absorption behaviour, and it could be comparable to granular material (Horoshenkov and Swift, 2001). Granular materials may be considered a particular case of porous materials, and their first peak of normal incidence sound absorption, f_0, can be described by Eq. 14:

$$f_0 = \frac{1}{2\pi} \sqrt{\frac{k}{M_{eff}}} \qquad (14)$$

where M_{eff} is the effective mass of granular material and k is the apparent dynamic longitudinal elastic modulus, detailed in past studies (Horoshenkov and Swift, 2001; Voronina and Horoshenkov, 2004). After the first peak, the composite behaviour was closer to the typical porous materials, with a slight increase in the sound absorption curve.

3.5. Air flow resistivity

Table 5 reports the results of air flow resistivity and the extended uncertainty for the three tested composite samples. As previously described, the test was carried out three times for each sample, by

Table 5
Results of air flow resistivity and the extended uncertainty for the three tested composite samples.

Composite samples	Air flow resistivity [kPa s/m²]	Extended uncertainty
A7	23.69	±0.57
A8	7.46	±0.18
A9	18.33	±0.55

placing the rougher side facing the environment and the flatter one facing the inside of the measurement tube.

The extended uncertainty was good, namely under 3%, but the reproducibility was relatively low. Further analysis could better explain these results. For example, the internal distribution of the voids, namely the tortuosity and porosity. Nevertheless, this information was considered and provided to better understand the acoustic properties.

3.6. Flexural strength

Fig. 6 shows the stress-strain curve. The dotted lines represent the samples placed in the Galdabini machine with the rougher side as the lower one (samples ROU_LOW); the continuous lines represent the samples with the rougher side as the upper one (samples ROU_UP). Table 6 reports the maximum force and displacement, the flexural strength, and the modulus of elasticity (considering the average values and standard deviation).

The bending behaviour was reported for all samples until achieving the maximum load (100 kN), as previously described (Section 3.5). Indeed, none achieved the rupture, and the test was performed up to the maximum capacity set in the machine. Fig. 7 shows four samples after the bending test.

The samples with the rougher side as the upper one (samples ROU_UP), having as the stressed side by the flexural stress the one with more amount of sodium silicate, demonstrated greater bending behaviour and higher flexural strength (Table 6). For them, both the maximum force and the flexural strength increased by 67%, while the modulus of elasticity, increased by 44%. The elongated shape of the giant reed with higher quantities of sodium silicate solution guaranteed high cohesion, thus good mechanical resistance and increased flexural strength. This could be an advantage for future applications as indoor coating insulation boards, although the applied load remained low if compared with structural composites.
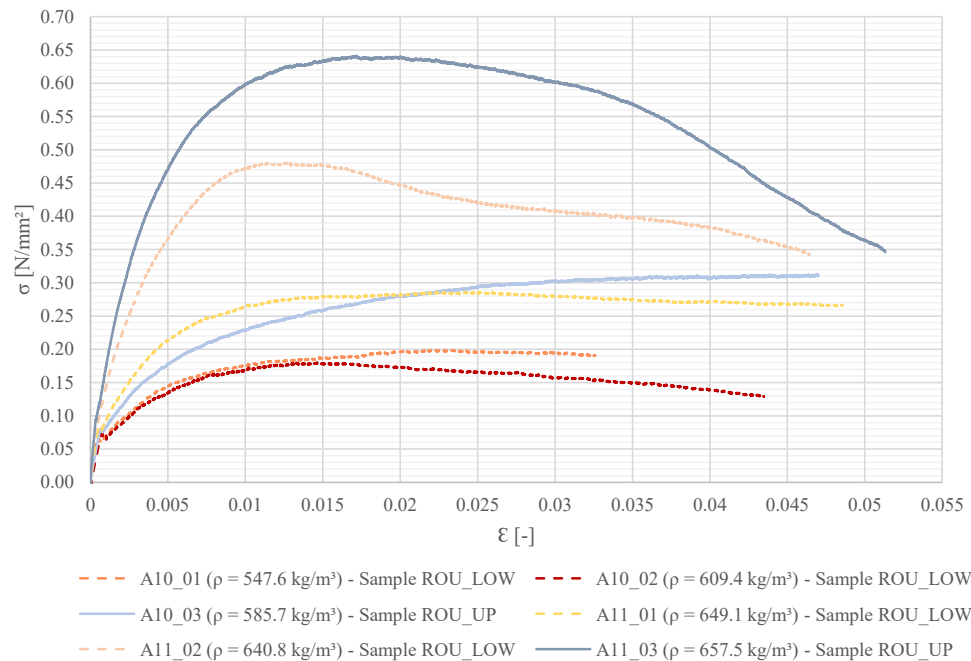
Fig. 6. Bending behaviour of the tested samples. The dotted lines represent the samples placed in the Galdabini machine with the rougher side as the lower one (samples ROU_LOW); the continuous lines represent the samples with the rougher side as the upper one (samples ROU_UP).

Table 6
Average values and standard deviation of maximum force, displacement, flexural strength, and modulus of elasticity for the bending test.

	F_{max} [N]	δ_{max} [mm]	σ_{max} [N/mm^2]	$E_{(20\%-60\%)}$ [N/mm^2]
Samples ROU_LOW	98.0 ± 43.6	16.3 ± 5.0	0.29 ± 0.14	41.8 ± 21.8
Samples ROU_UP	148.7 ± 63.3	29.2 ± 18.4	0.48 ± 0.23	60.4*
All	114.9 ± 51.2	20.6 ± 11.3	0.35 ± 0.18	48.0 ± 30.1

Note: *The S.D. was not calculated for Samples ROU_UP because only two samples were considered and reported.

Fig. 7. Four samples (10 cm × 50 cm × 4 cm) of giant reed and sodium silicate solution after the bending test.

3.7. Compressive strength

Fig. 8 reports the stress-strain graph, showing the compressive behaviour of the samples until 10% strain.

Table 7 reports the average values and standard deviation of the force at 10% strain (F_{10}) and the corresponding displacement (δ_{10}), the compressive strength (σ_{10}), and the modulus of elasticity (E_{10}), calculated as reported in Eq. 9.

The compressive behaviour did not show a peak and then a collapse: the samples did not achieve the yield. The samples were pressed and flattened, and the test stopped at the set maximum load (100 kN). For this reason, according to EN 826 (EN 826:2013), compressive strength and the corresponding force were determined by considering 10% strain ($\epsilon = 0.1$), as described in Section 2.3.

Fig. 9 shows the stress-strain curve, considering all the compressive test performance times.

The compressive test results allowed making important considerations, both on materials' behaviour (giant reed, sodium silicate solution, and their mixture) and on feasible production processes, namely by pressing the composites, as detailed in the following section. The composite did not achieve the yield, but it flattened. Fig. 10 reports an example of two tested samples, before and after the test.

4. Discussion

4.1. Comparison with past studies

The results of each property were compared with literature values and commercial products to validate and discuss them. It is essential to underline that the values considered for the comparison could be determined in different laboratory conditions, for different shape and size samples, and by other test methods. Although the present study evaluated the giant reed as a particle aggregate, bio-wastes and bio-resources employed as fibres and particles were considered. This
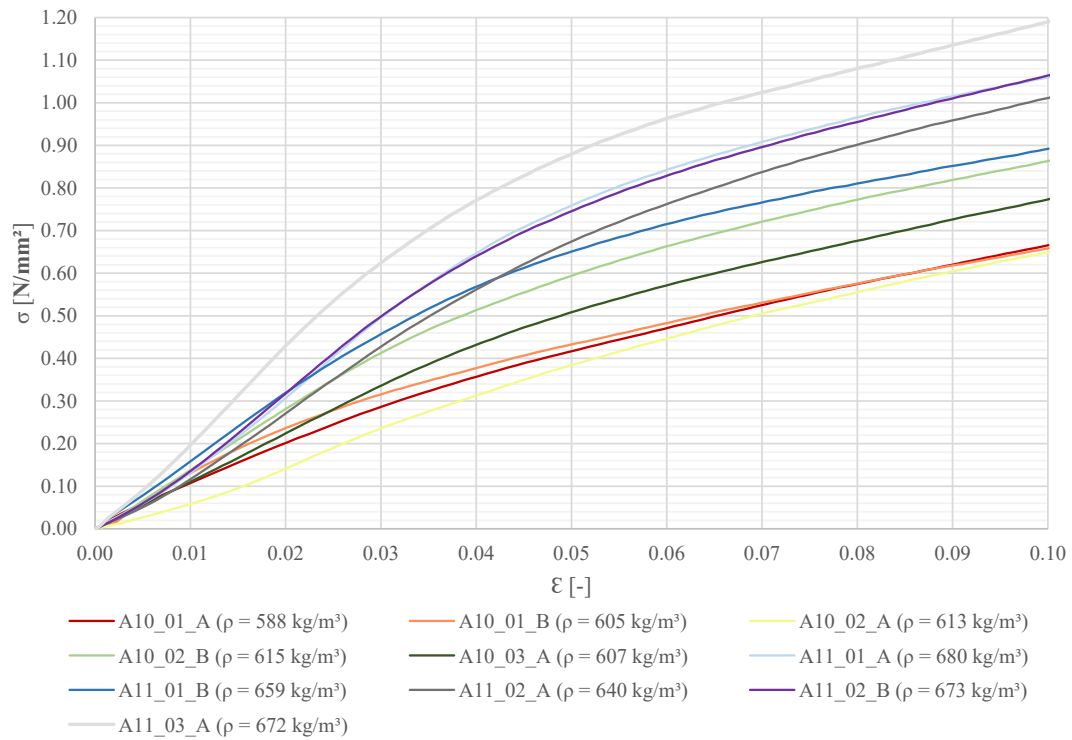
Fig. 8. Compressive behaviour of the tested composite samples: stress-strain graphic until 10% strain.

Table 7
Average values and standard deviation of the tested samples: maximum force and displacement, compressive strength, and modulus of elasticity.

F_{10} [N]	δ_{10} [mm]	σ_{10} [N/mm^2]	$E_{(20\%-60\%)}$ [N/mm^2]
8932 ± 1929	3.7 ± 0.1	0.9 ± 0.2	13.0 ± 4.3

enriched the considerations, showing how bio-based composites could result in building products with different properties.

Fig. 11 shows the correlation between thermal conductivity and apparent density of the giant reed-based composite and some literature values, better detailed in Cintura et al. (Cintura et al., 2023a).

The composite of giant reed and the sodium silicate solution showed values of apparent density higher than all the ones considered for
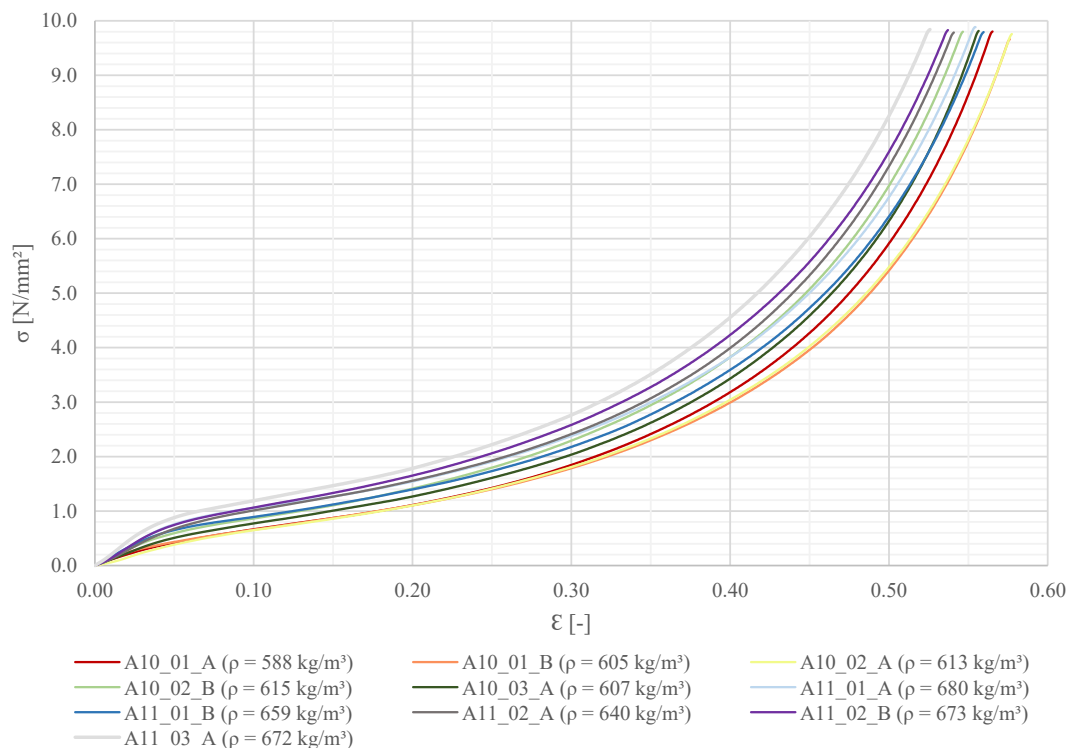

Fig. 9. Compressive behaviour of the tested composite samples: stress-strain graphic until reaching the maximum capacity.

Fig. 10. Example of two giant reed-based composite samples employed for the compressive test before (left) and after the compressive test (right).
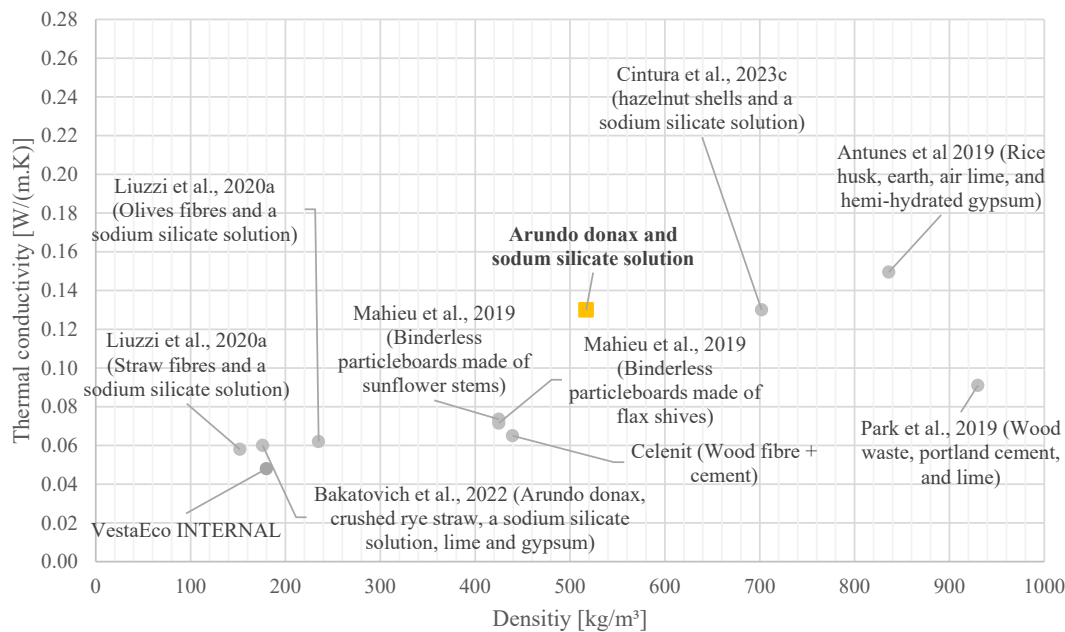

Fig. 11. Correlation between thermal conductivity and apparent density of the studied composite compared with literature values and commercial products reported in (Cintura et al., 2023a).

comparison, except for the boards made of rice husk, earth, air lime, and hemi-hydrated gypsum (Antunes et al., 2019), boards made of wood waste, Portland cement, and lime (Park et al., 2019), and a composite of hazelnut shells and sodium silicate (produced with the same production process and percentages of aggregate-adhesive (Cintura et al., 2023c)). As for the thermal properties, the giant reed-based composite had values of thermal conductivity similar to the hazelnut shells-based one (Cintura et al., 2023c), lower than rice husk-based boards (Antunes et al., 2019), and higher than the others considered composites.

As previously mentioned, it is essential to underline that, even if all the compared products were bio-based, some of them were produced by using fibres instead of particles. This resulted in lower density and better thermal insulation performance (Cintura et al., 2021; Panyakaew and Fotios, 2011).

The result of the comparison was in line with the expectation. The commercial products, namely thermal and acoustic insulation Celenit N boards made of mineralized wood wool and Portland cement (Celenit, 2022), and internal boards composed of lignocellulosic fibres and PMDI resin VestaEco (Vestaeco, 2022), were optimized to meet the requirements to be used as insulators. Mahieu et al. (Mahieu et al., 2019) did not use any binder. Hence, the final properties depended on the production process and the fibres (light materials with good thermal performance). Park et al. (Park et al., 2019) considered wood waste (light aggregate) and an optimized mix design. Antunes et al. (Antunes et al., 2019) achieved higher density and thermal conductivity values, probably due to the clay-based binding matrix. As for the composites with sodium silicate solution, Liuzzi et al. (Liuzzi et al., 2020a)

considered both lighter aggregates and lower amounts of sodium silicate solution. Bakatovich et al. (Bakatovich et al., 2022) achieved lower thermal conductivity values for *A. donax*-based composites bounded by sodium silicate with lime and gypsum thanks to the addition of ray straw. Indeed, by replacing the *A. donax* with straw, the thermal insulation capacity of the mixture of the two aggregates (without any binders) improved. Cintura et al. (Cintura et al., 2023c), achieved higher values of both density and thermal conductivity for the hazelnut shells-based composites, due to the selected aggregates, with higher loose bulk density – (469.3 ± 5.8) kg/m³ –.

Considering the reference values to define a material as a thermal insulator, namely 0.065 W/(m.K) (Pina dos Santos and Matias, 2006; Romano et al., 2019), even if some part studies reported 0.1 W/(m.K) (Martínez-García et al., 2020; Mati-Baouche et al., 2014), the composite cannot be considered as such, even if good thermal insulation properties were expected from giant reed (Barreca, 2012; Carneiro et al., 2016; Malheiro et al., 2021).

Fig. 12 shows the comparison between the results of the hygroscopicity analysis for the giant reed-based composite and the hazelnut shells-based one (average values and standard deviation of the analysed samples), evaluated by Cintura et al. (Cintura et al., 2023c).

The production process, aggregates-adhesive percentages, and the tested method of the two composites were the same. Hence, the differences derived from the bio-aggregates (physical and chemical properties), and the different distribution of the sodium silicate solution in the adsorbing/desorbing surface. Fig. 12 demonstrates that the giant reed-based composite had greater moisture storage capacity than the
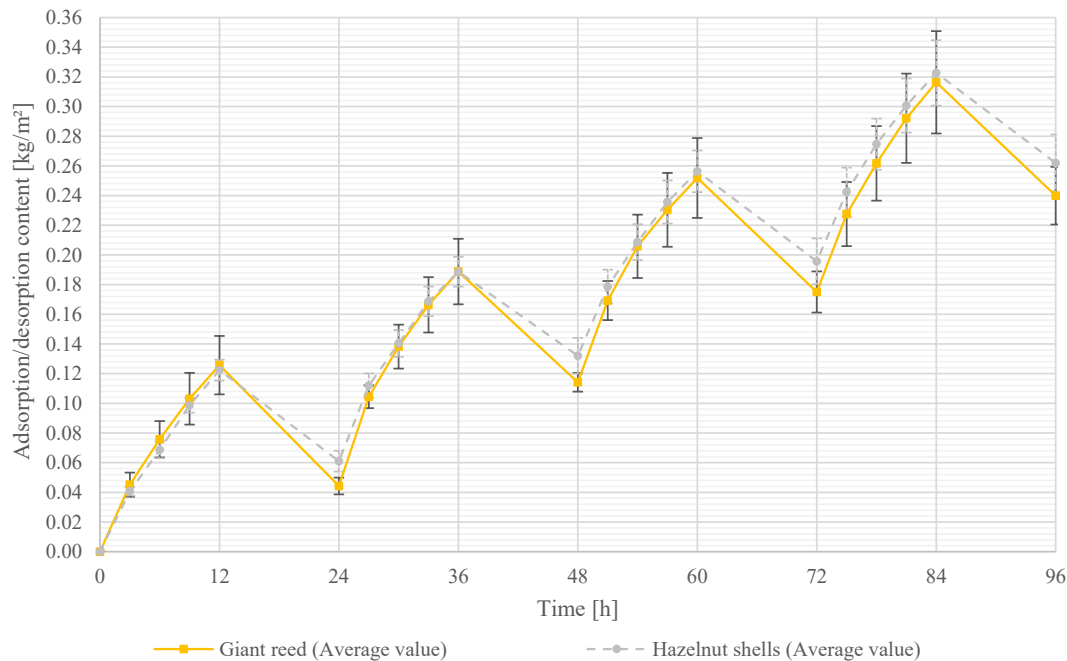
Fig. 12. Moisture adsorption/desorption content for four cycles: comparison between the average value of the tested giant reed-based composite samples and hazelnut shell-based ones, evaluated by Cintura et al. (Cintura et al., 2023c).

hazelnut shell-based one (considering the standard deviations). This could be caused by an excess sodium silicate solution on the giant reed-based samples' surface, determined by the employed method. However, the hygroscopicity behaviour was almost the same, as well as the moisture content. The maximum values of moisture content were $\rho_{(A,ac)}$ = 0.14 kg/m^2 and $\rho_{(A,dc)}$ = 0.08 kg/m^2 for the giant reed-based composite, $\rho_{(A,ac)}$ = 0.12 kg/m^2 and $\rho_{(A,dc)}$ = 0.06 kg/m^2 for the hazelnut shells-based. Both showed high hygroscopicity compared with a past study (Cintura et al., 2023a). This result also confirmed the sodium silicate solution's hygroscopic properties (Lee and Thole, 2018; Song et al., 2021).

The comparison of the MBV – (4.33 ± 1.84) g/(m^2 %RH) – with already cited past studies that employed the sodium silicate solution as the adhesive demonstrated that the results were coherent with the literature. Liuzzi et al. (Liuzzi et al., 2020a) reported values of the ideal MBV of 5.05 g/(m^2 %RH) for composites made up of straw fibres and sodium silicate solution, and 3.29 g/(m^2 %RH), for olive fibres and the sodium silicate solution. Practical MBV and ideal MBV are similar in the case of homogeneous composites and if the penetration depth is less or equal to the samples' thickness (Rode et al., 2005). Cintura et al. (Cintura et al., 2023c) reported MBV of (3.45 ± 1.76) g/(m^2 %RH) for hazelnut shells and sodium silicate solution (calculated considering the same conditions as the present study).

Composites as similar as possible to giant reed-based ones were considered to compare and discuss the acoustic results, namely made of bio-wastes employed as particles rather than fibres. A composite made of olive pruning waste and chitosan dissolved in acetic acid and water as a binder had a sound absorption curve similar to the one of giant reed-based with a peak at higher frequencies (Martellotta et al., 2018). The same results were achieved for a composite made of sunflower stalks and chitosan (Mati-Baouche et al., 2016). Hazelnut shells-based boards with sodium silicate solution (Cintura et al., 2023c) showed the same acoustic absorption behaviour. The same adhesive and production process resulted in stiff samples with internal cavities. The main difference was the second slight increase of the curve after the first peak (Fig. 5), in the case of the giant reed-based composite, more similar to porous materials. For the hazelnut shell-based composite the sound absorption coefficient achieved the higher values at frequencies between 700 Hz and

900 Hz, while for the giant reed-based one was between 600 Hz and 700 Hz. In both cases, this frequency range was in the one of the human voice, between 500 Hz and 1000 Hz (EN IEC 60268–16:2020; ISO 3382–3:2012). Further analyses should be carried out since a combination of the two bio-aggregates may determine an increment of the amplitude of the peak, hence of the frequency range. The mixture of round-shaped aggregates (from hazelnut) with elongated ones and the sodium silicate solution could result in a sound absorber with even more advantageous behaviour.

Glé et al. (Glé et al., 2011) reported the acoustic absorption of hemp shiv analysed as raw material. They marked the influence of the particle size, concluding that the smaller ones, the better sound absorption, especially for low frequencies. The acoustic absorption curve was similar to the one of the giant reed-based composite. Indeed, the first peak in the absorption curve occurred around 600 Hz; then, a second peak at 1700 Hz. For the giant reed-based composite, the second peak was not so evident; in this case, the sound absorption curve increased. Kinnane et al. (Kinnane et al., 2016), reporting the sound absorption curve of the hemp shiv as raw materials, showed similar behaviour. The researchers highlighted the importance of the particles' compaction.

Even if these examples referred to the sound absorption performance of the raw materials, they provided helpful information for further analysis. Moreover, they demonstrated that the sound absorption performance of giant reed-based composite was probably due to aggregate shapes, compaction, and dispositions, which produced voids in the samples' surface and internal layer.

Finally, the comparison was carried out for the results of mechanical tests. Ng et al. (Ng et al., 2018) considered boards made up of shredded sugarcane bagasse and a sodium silicate solution in different percentages. The researchers reported higher flexural strength values, between 15.40 N/mm^2 and 21.19 N/mm^2, probably due to the production process, which consisted of hot pressing and determined higher density. They concluded that a higher amount of sodium silicate improved the flexural strength. Savic et al. (Savic et al., 2020) investigated the properties of composites made of *Miscanthus x giganteus* fibres, mineral binders (based on cement and hydrated lime), and pozzolanic materials. They tested prismatic samples and reported flexural strength values between 0.11 N/mm^2 and 0.63 N/mm^2 (more similar to the ones

achieved for giant reed), varying depending on the considered binder. Mathews et al. (Mathews et al., 2023) tested insulation panels made up of recycled cardboard as aggregates and different binders. They achieved values of flexural strength between 0.11 N/mm^2 and 0.36 N/mm^2 for lime-based binder and boric acid, and between 0.34 N/mm^2 and 0.91 N/mm^2 for clay-based one (again, more comparable to giant reed's ones).

The comparison with the reference past study using hazelnut shells as aggregates showed interesting results. The composite evaluated by Cintura et al. (Cintura et al., 2023c) had a different behaviour: the strain-stress curve represented an initial elastic behaviour, then the achievement of a maximum load (peak). As all the other parameters were kept identical, the differences were caused by the physical and chemical characteristics of the aggregates and the physical properties derived from the mixture aggregates-adhesive. In addition to its greater mechanical properties (Carneiro et al., 2016; Molari et al., 2021), the elongated and flattened shape of the giant reed guaranteed more cohesion between the particles and the sodium silicate solution, which widely influenced the final performance (Ng et al., 2018). As for the numerical values, the results were similar, since for the hazelnut shells-based composite were $\sigma_{max} = (0.43 \pm 0.04)$ N/mm^2, when the rougher side was the upper one, $\sigma_{max} = (0.35 \pm 0.04)$ N/mm^2 when it was the lower one, and $\sigma_{max} = (0.39 \pm 0.06)$ N/mm^2 as the average value of all the tested samples. For the giant reed-based composite, the sodium silicate solution's distribution influenced the flexural strength more than the hazelnut shells-based one.

As for the compressive behaviour, the composite made up of giant reeds showed a stress-strain curve similar to straw bales (Maraldi et al., 2017, 2016; Molari et al., 2017). This result was considered to select the compared reference studies. Barbieri et al. (Barbieri et al., 2020) regarded composites of hemp and wheat husk as aggregate and a mixture of lime putty and natural hydraulic lime as a binder (called lime hemp and lime wheat husk concrete, respectively). Lime wheat husk concrete showed a compressive behaviour similar to the giant reed-based composite and a compressive strength of (0.16 ± 0.02) N/mm^2. As for the lime hemp concrete, a value of (0.24 ± 0.03) N/mm^2 was determined. Savic et al. (Savic et al., 2020) for prismatic samples of *Miscanthus x giganteus* fibres, mineral binders (based on cement and hydrated lime), and pozzolanic materials reported values between 0.139 N/mm^2 and 1.349 N/mm^2, depending on the binder. Celenit N (Celenit, 2022) at 10% deformation demonstrated compressive stress higher or equal to 0.2 N/mm^2, for thickness between 15 mm and 40 mm. These comparisons revealed that the results were consistent with the literature. Moreover, although the giant reed-based composite did not show enough mechanical resistance to be employed as a structural material, it demonstrated promising performance, especially for compressive strength.

The compression test showed another feasible, maybe more efficient, production process: pressing the mixture of giant reed and sodium silicate solution. As a first characterization, the apparent density (average value of all the tested samples) was calculated before and after the test. Consistently with the expectation, it increased, by 19%. Further analysis should be carried out to determine how a pressing process could change the composite's final properties.

4.2. Implications and explanations of the results

The analysis of the results and the comparison with past studies ensured essential considerations. First, the thermal analysis demonstrated the significant influence of the selected adhesive/binder on the final composite's performance (Cintura et al., 2023a). Although the promising thermal properties of the considered bio-aggregate, the composite did not result in a low thermal insulation product (assuming the standard requirement for these insulators). The influence of the adhesive was clear also in hygroscopicity, even if it is less influencing. In this case, the results were determined by both the giant reed and the

sodium silicate. To further investigate the influence of each material, laboratory tests could be performed by considering them separately (i.e., the aggregates, the sodium silicate, and the composite).

The acoustic behaviour seemed to be determined mainly by the final configurations of the composite (stiffness with voids). Indeed, the results of the giant reed-based composite and the hazelnut shells-based one were highly similar. Past studies that evaluated raw materials' acoustic behaviour (Kinnane et al., 2016; Glé et al., 2011) suggested that the sound absorption curve of the aggregates (as raw materials, without any binders) might be similar. Thus, bonding them by keeping them in a similar configuration to the one they had as raw materials, might be the solution to have this acoustic performance. The present study ensured this by the sodium silicate solution, mixed without pressing. However, again, an analysis of the materials considered separately (i.e., aggregates, adhesive, and composite) would be helpful to support this consideration. Finally, the result of the air flow resistivity suggested that further analysis of the internal distribution of voids (porosity and tortuosity) might be performed. This analysis could be a starting point for future studies, focused on the deep investigation of acoustic properties.

The mechanical performance was provided by both the aggregate and the mixture aggregates-adhesive. In addition to the giant reed's excellent mechanical properties (Molari et al., 2021), the aggregates' elongated shape and the sodium silicate solution with the production process, ensured good cohesion. This aspect avoided the samples' yield and improved the mechanical resistance. Although the composite cannot be used for structural purposes, the results were extremely interesting, especially for the compressive strength. They outlined a production process that might produce a stronger and more mechanically performing composite.

4.3. Benefits, drawbacks, and possible applications

The study demonstrated the several benefits of the analysed composite. First, the sustainable aspects, that were guaranteed by the selected materials. As past studies reported (Mahieu et al., 2019; Rubino et al., 2023), being *A. donax* an abundant, renewable, and perennial by-product, the energy consumption derived from the production process could be considered negligible. The sodium silicate solution may have a higher environmental impact. Still, it enabled the use of low temperatures during the casting and curing phases, lowering the energy consumption during the production process. Furthermore, confirming the information provided by past research (Lee and Thole, 2018; Liuzzi et al., 2020a), it moderated some of the main drawbacks of using bio-wastes, namely the resistance against biological attacks, avoiding any biological colonization (even after the hygroscopic tests). Finally, the sodium silicate solution was considered a non-toxic adhesive, not harmful to human health. These qualitative considerations indicate that various aspects made the composite eco-efficient, but a quantitative evaluation (e.g., life cycle assessment) should be carried out.

Considering the evaluated properties, the main advantages of the proposed composite are derived from acoustic absorption (absorbing the frequencies of human noise sources) and hygroscopic moisture buffering capacity. It is expected that giant reed-based boards can be suitable in environments where the speech and the involuntary listening of the users can cause acoustic discomfort (e.g., restaurants, offices, lecture halls, or museums (Cingolani et al., 2021; D'Orazio et al., 2020; De Salvio et al., 2021)). The high hygroscopicity and the high moisture buffering capacity can passively contribute to indoor conditions control. Hence, the results suggested a suitable composite's employment as internal coating boards to improve hygrothermal and acoustic comfort. However, the resistance to fire should be assessed to provide further support to this consideration.

Further analysis of the acoustic properties could be performed, both to better understand the giant reed-based composite behaviour and to propose an optimization. Since the acoustic absorption capacity is strongly related to the thickness, tortuous morphology, and pore

structure (Asdrubali et al., 2016; Liuzzi et al., 2020b), the internal structure could be analysed. Regarding the possible optimization, as previously mentioned, the amplitude of the curve generated by the absorption peak should be increased, guaranteeing an absorption coefficient $\alpha \approx 1.00$ for a broader range of frequencies. Finally, an interesting possibility to explore could be the combination of the considered giant reed-based boards with Mass-Loaded Vinyl (MLV) panels or barriers. They consist of effective sound-blocking products due to their resonant capacity, employed in walls, ceilings, and floors (Commercial-Acoustics, 2023; Gupta, 2019). Combining these two products (e.g., applying an MLV barrier in one face of the giant reed-based boards) might result in an optimized, more performant acoustic absorber. As past research demonstrated (O'Flaherty and Alam, 2021), MLV barriers could improve boards' sound absorption performance. Furthermore, the MLV could moderate one of the possible drawbacks of bio-based composites, namely the easy degradation and the low durability (Cintura et al., 2021).

The high hygroscopicity could be both an advantage and a disadvantage, securing a passive control of indoor conditions and causing composite's degradation. High moisture content could modify the materials' properties and make them more susceptible to biological attack (Esteves et al., 2021; Krejsová and Doleželová, 2019; Verdier et al., 2014). Nevertheless, considering, in general, the low resistance to biological attack of agro-industrial wastes, the results of the visual observation after the hygroscopicity test were promising, confirming one of the benefits of using the sodium silicate solution. In addition to the contribution of the giant reed and the sodium silicate solution, separately (Section 4.2), it could be interesting to evaluate the influence of moisture content on the other properties, perform the hygroscopicity test for more than four cycles, and determine the possible critical moisture levels (Johansson et al., 2020).

Even if the thermal analysis results demonstrated that the giant reed-based composite cannot be considered a thermal insulator, this property could probably be improved by changing some parameters (e.g., the grain size, the percentages of aggregates-adhesive, and the production process). However, the composite could be employed as coating boards with some thermal insulation capacity. The influence of RH on thermal conductivity could be further analysed, as they are strictly related (Cintura et al., 2022; Liuzzi et al., 2017). This study was not carried out in the present work, as a detailed thermal performance evaluation was not one of the main aims. Furthermore, the low-promising performance did not encourage further analysis of this property. Lower thermal conductivity values could be achieved at lower values of RH, but much lower levels would not represent the indoor conditions.

Finally, as the compressive test demonstrated, pressing the composite was a feasible production process. Maybe, even if this would determine higher energy demand, it could improve giant-reed-based boards' properties.

5. Conclusions

This study analysed the properties of a composite of bio-waste-aggregates, namely particles of giant reed (*Arundo donax* L.) and a sodium silicate solution. Apparent density, thermal conductivity, sound absorption, and flexural and compressive strength were evaluated to provide a wide-range characterization of the unconventional composite. The outcomes helped define the giant reed-based composite's most promising properties and support de decision to carry out future studies on producing eco-efficient boards. A comparison with the literature was carried out to understand better, discuss, and validate the results.

The achieved conclusions are reported below.

- The production process, as well as the mix design (percentage aggregates-adhesive), could be optimized, for example, by using less amount of sodium silicate solution or pressing the mixture of

materials. Furthermore, future studies could evaluate the influence of the aggregates' particle size on the composite's final properties.
- The tested composite had higher values of apparent density and, coherently, higher thermal conductivity values than the composites considered for comparison. The composite did not meet the standard requirements to be classified as a thermal insulator. Still, the thermal performance may be improved by modifying some production parameters, as good thermal insulation capacity was expected from *A. donax*. Furthermore, the correlation between thermal conductivity and RH could be analysed.
- The composite showed high hygroscopicity, probably mainly determined by the sodium silicate solution, but the giant reed contributed to the moisture storage capacity. The moisture buffering value is in line with literature values and the composite showed high moisture buffering capacity, which could be both a benefit and a drawback. Even after the hygroscopicity test, no mould growth was detected. Hence, the composite did not show increased susceptibility to biological attack.
- The sound absorption behaviour was not so typical, considering bio-waste-based boards already studied, and it was typical of granular materials. The highest sound absorption coefficient values were achieved for frequencies between 600 Hz and 700 Hz, which was in the frequency range of the human voice. Hence, possible employment of the giant reed-based composite could be as indoor coating boards with acoustic absorption capacity. Further investigation could better explain the composite's behaviour and provide optimization, by enlarging the frequency range with a high acoustic absorption coefficient.
- The mechanical performance was inadequate for using the giant reed-based composite as structural boards or masonry units. The composite did not reach a rupture load, both for the bending and compressive test, and the amount and the distribution of the sodium silicate solution influenced the flexural strength values. The compressive performance was higher than other bio-based composites considered for comparison. Furthermore, the performed analysis demonstrated the feasibility of producing a giant reed composite by pressing the materials and suggested ideas for future studies.

The laboratory tests to analyse the properties of boards made up of giant reed and sodium silicate solution demonstrated their promising use as sustainable internal coating boards, that would be not toxic for human health, and able to control acoustic and hygrothermal indoor comfort.

Further studies could be carried out on the already analysed properties and new ones. Indeed, the present work wanted to provide a general characterization of the composite as a starting point for further studies. The most promising aspects, namely the hygroscopicity and the acoustic performance, should be further evaluated by a vertical analysis. Hence, these properties could be optimized. Furthermore, a life cycle analysis is needed to quantify the eco-efficiency of this bio-waste-based building solution, as well as the evaluation of composite's degradation (e.g., resistance to biological attack and reaction to fire).

CRediT authorship contribution statement

Eleonora Cintura: Conceptualization, Investigation, Formal analysis, Data curation, Methodology, Visualization, Validation, Writing – original draft. **Paulina Faria:** Conceptualization, Writing – review & editing, Supervision, Funding acquisition, Project administration. **Luisa Molari:** Conceptualization, Investigation, Writing – review & editing, Supervision. **Luca Barbaresi:** Conceptualization, Investigation, Writing - review & editing. **Dario D'Orazio:** Conceptualization, Investigation, Writing – review & editing. **Lina Nunes:** Conceptualization, Writing – review & editing, Supervision, Funding acquisition, Project administration.

Declaration of Competing Interest

Data Availability

Data will be made available on request.

Acknowledgements

References

Alexopoulou, E., Zanetti, F., Scordia, D., Zegada-Lizarazu, W., Christou, M., Testa, G., Cosentino, S.L., Monti, A., 2015. Long-term yields of switchgrass, giant reed, and miscanthus in the Mediterranean Basin. BioEnergy Res. 8, 1492–1499. https://doi.org/10.1007/s12155-015-9687-x.

Amziane, S., Collet, F., Lawrence, M., Magniont, C., Picandet, V., Sonebi, M., 2017. Recommendation of the RILEM TC 236-BBM: characterisation testing of hemp shiv to determine the initial water content, water absorption, dry density, particle size distribution and thermal conductivity. Mater. Struct. 50, 167. https://doi.org/10.1617/s11527-017-1029-3.

Ansell, M.P., Lawrence, M., Jiang, Y., Shea, A., Hussain, A., Calabria-Holley, J., Walker, P., 2020. Natural plant-based aggregates and bio-composite panels with low thermal conductivity and high hygrothermal efficiency for applications in construction. Nonconventional and Vernacular Construction Materials. Elsevier,, pp. 217–245. https://doi.org/10.1016/B978-0-08-102704-2.00010-X.

Antunes, A., Faria, P., Silva, V., Brás, A., 2019. Rice husk-earth based composites: a novel bio-based panel for buildings refurbishment. Constr. Build. Mater. 221, 99–108. https://doi.org/10.1016/j.conbuildmat.2019.06.074.

Asdrubali, F., Bianchi, F., Cotana, F., D'Alessandro, F., Pertosa, M., Pisello, A.L., Schiavoni, S., 2016. Experimental thermo-acoustic characterization of innovative common reed bio-based panels for building envelope. Build. Environ. 102, 217–229. https://doi.org/10.1016/j.buildenv.2016.03.022.

ASTM C522–03:2022, 2022. Standard Test Method for Airflow Resistance of Acoustical Materials. Pennsylvania, PA, USA.

Auriga, R., Pędzik, M., Mrozowski, R., Rogoziński, T., 2022. Hemp shives as a raw material for the production of particleboards. Polymers 14, 5308. https://doi.org/10.3390/polym14235308.

de Azevedo, A.R.G., Amin, M., Hadzima-Nyarko, M., Saad Agwa, I., Zeyad, A.M., Tayeh, B.A., Adesina, A., 2022. Possibilities for the application of agro-industrial wastes in cementitious materials: a brief review of the Brazilian perspective. Clean. Mater. 3, 100040 https://doi.org/10.1016/j.clema.2021.100040.

Bakatovich, A., Gaspar, F., Boltrushevich, N., 2022. Thermal insulation material based on reed and straw fibres bonded with sodium silicate and rosin. Constr. Build. Mater. 352, 129055 https://doi.org/10.1016/j.conbuildmat.2022.129055.

Baldinelli, G., Bianchi, F., Gendelis, S., Jakovics, A., Morini, G.L., Falcioni, S., Fantucci, S., Serra, V., Navacerrada, M.A., Díaz, C., Libbra, A., Muscio, A., Asdrubali, F., 2019. Thermal conductivity measurement of insulating innovative building materials by hot plate and heat flow meter devices: a round robin test. Int. J. Therm. Sci. 139, 25–35. https://doi.org/10.1016/j.ijthermalsci.2019.01.037.

Barbieri, V., Lassinantti Gualtieri, M., Siligardi, C., 2020. Wheat husk: a renewable resource for bio-based building materials. Constr. Build. Mater. 251, 118909 https://doi.org/10.1016/j.conbuildmat.2020.118909.

Barreca, F., 2012. Use of giant reed *Arundo donax* L. in rural constructions. Agric. Eng. Int.: CIGR J. 14, 46–52.

Berzborn, M., Bomhardt, R., Klein, J., Richter, J.-G., Vorländer, M., 2017. The ITA-Toolbox: An Open Source MATLAB Toolbox for Acoustic Measurements and Signal Processing, in: Fortschritte Der Akustik - DAGA 2017, 43. Deutsche Jahrestagung Für Akustik. Kiel, pp. 222–225.

Caponetto, R., Cuomo, M., Detommaso, M., Giuffrida, G., Presti, A.Lo, Nocera, F., 2023. Performance assessment of giant reed-based building components. Sustainability 15, 2114. https://doi.org/10.3390/su15032114.

Carneiro, P., Jerónimo, A., Silva, V., Cartaxo, F., Faria, P., 2016. Improving building technologies with a sustainable strategy. Procedia - Soc. Behav. Sci. 216, 829–840. https://doi.org/10.1016/j.sbspro.2015.12.080.

de Carvalho, P.S., Nora, M.D., da Rosa, L.C., 2020. Development of an acoustic absorbing material based on sunflower residue following the cleaner production techniques. J. Clean. Prod. 270, 122478 https://doi.org/10.1016/j.jclepro.2020.122478.

Celenit, Celenit N, (2022). https://www.celenit.com/en-UK/celenit-n.php (last accessed 03.16.2022).

Ceotto, E., Vasmara, C., Marchetti, R., Cianchetta, S., Galletti, S., 2021. Biomass and methane yield of giant reed (Arundo donax L.) as affected by single and double annual harvest. GCB Bioenergy 13, 393–407. https://doi.org/10.1111/gcbb.12790.

Chastre, C., Faria, P., Neves, J., Ludovico-Marques, M., Biscaia, H., Nunes, L., 2023. Innovative durability tests on construction materials. In: Advances on Testing and Experimentation in Civil Engineering. Springer, Cham, pp. 53–73. https://doi.org/10.1007/978-3-031-23888-8_3.

Chung, J.Y., Blaser, D.A., 1980a. Transfer function method of measuring in-duct acoustic properties. II. Exp. J. Acoust. Soc. Am. 68, 914–921. https://doi.org/10.1121/1.384779.

Chung, J.Y., Blaser, D.A., 1980b. Transfer function method of measuring in-duct acoustic properties. I. Theory. J. Acoust. Soc. Am. 68, 907–913. https://doi.org/10.1121/1.384778.

Cingolani, M., Fratoni, G., Barbaresi, L., D'Orazio, D., Hamilton, B., Garai, M., 2021. A trial acoustic improvement in a lecture Hall with MPP sound absorbers and FDTD acoustic simulations. Appl. Sci. 11, 2445. https://doi.org/10.3390/app11062445.

Cingolani, M., Fusaro, G., Fratoni, G., Garai, M., 2022. Influence of thermal deformations on sound absorption of three-dimensional printed metamaterials. J. Acoust. Soc. Am. 151, 3770–3779. https://doi.org/10.1121/10.0011552.

Cintura, E., Molari, L., Barbaresi, L., D'Orazio, D., Faria, P., Nunes, L., 2023c. Hazelnut shells as high mass bio-aggregates in building composites: hygrothermal, acoustic, and mechanical performance. submitted for publication to Journal of Cleaner Production.

Cintura, E., Nunes, L., Esteves, B., Faria, P., 2021. Agro-industrial wastes as building insulation materials: a review and challenges for Euro-Mediterranean countries. Ind. Crops Prod. 171, 113833 https://doi.org/10.1016/j.indcrop.2021.113833.

Cintura, E., Faria, P., Duarte, M., Nunes, L., 2022. Bio-Wastes as aggregates for eco-efficient boards and panels: screening tests of physical properties and bio-susceptibility. Infrastructures 7, 26. https://doi.org/10.3390/infrastructures7030026.

Cintura, E., Faria, P., Duarte, M., Nunes, L., 2023a. Eco-efficient boards with agro-industrial wastes – assessment of different adhesives. Constr. Build. Mater. 404, 132665 https://doi.org/10.1016/j.conbuildmat.2023.132665.

Cintura, E., Faria, P., Molari, L., Nunes, L., 2023b. Optimisation of production parameters to develop innovative eco-efficient boards. In: Amziane, S., Merta, I., Page, J. (Eds.), Bio-Based Build. Mater. Proc. ICBBM 2023 111–122. https://doi.org/10.1007/978-3-031-33465-8_10.

Commercial-Acoustics, 2023. Technical Data - Commercial Acoustics Sound Barrier [WWW Document]. URL https://commercial-acoustics.com/ (accessed 9.11.23).

Corredor-Bedoya, A.C., Acuña, B., Serpa, A.L., Masiero, B., 2021. Effect of the excitation signal type on the absorption coefficient measurement using the impedance tube. Appl. Acoust. 171, 107659 https://doi.org/10.1016/j.apacoust.2020.107659.

D'Orazio, D., Montoschi, F., Garai, M., 2020. Acoustic comfort in highly attended museums: a dynamical model. Build. Environ. 183, 107176 https://doi.org/10.1016/j.buildenv.2020.107176.

Danelli, T., Sepulcri, A., Masetti, G., Colombo, F., Sangiorgio, S., Cassani, E., Anelli, S., Adani, F., Pilu, R., 2021. Arundo donax L. biomass production in a polluted area: effects of two harvest timings on heavy metals uptake. Appl. Sci. 11, 1147. https://doi.org/10.3390/app11031147.

De Salvio, D., D'Orazio, D., Garai, M., 2021. Unsupervised analysis of background noise sources in active offices. J. Acoust. Soc. Am. 149, 4049. https://doi.org/10.1121/10.0005129.

De Salvio, D., Bianco, M.J., Gerstoft, P., D'Orazio, D., Garai, M., 2023. Blind source separation by long-term monitoring: a variational autoencoder to validate the clustering analysis. J. Acoust. Soc. Am. 153, 738–750. https://doi.org/10.1121/10.0016887.

Dennis, J., Nunes, L., Duarte, S., 2021. The application of bicine or tricine for limiting termite attack of thermally modified wood, in: InnoRenew CoE International Conference. Online, p. 31.

Echeverria, C.A., Ozkan, J., Pahlevani, F., Willcox, M., Sahajwalla, V., 2021. Effect of hydrothermal hot-compression method on the antimicrobial performance of green building materials from heterogeneous cellulose wastes. J. Clean. Prod. 280, 124377 https://doi.org/10.1016/j.jclepro.2020.124377.

EN 12667:2001, 2001. Thermal performance of building materials and products - Determination of thermal resistance by means of guarded hot plate and heat flow meter methods - Products of high and medium thermal resistance. European Committee for Standardization, CEN. Brussels, Belgium.

EN 323:1993, 1993. Wood-based panels - Determination of density. European Committee for Standardization, CEN. Brussels, Belgium.

EN 826:2013, 2013. Thermal insulation products for building applications - Determination of Compression Behaviour. European Committee for Standardization, CEN. Brussels, Belgium.

Esteves, B., Ferreira, H., Viana, H., Ferreira, J., Domingos, I., Cruz-Lopes, L., Jones, D., Nunes, L., 2021. Termite resistance, chemical and mechanical characterization of paulownia tomentosa wood before and after heat treatment. Forests 12, 1114. https://doi.org/10.3390/f12081114.

Faruk, O., Bledzki, A.K., Fink, H.-P., Sain, M., 2012. Biocomposites reinforced with natural fibers: 2000–2010. Prog. Polym. Sci. 37, 1552–1596. https://doi.org/10.1016/j.progpolymsci.2012.04.003.

Fiore, V., Scalici, T., Valenza, A., 2014. Characterization of a new natural fiber from Arundo donax L. as potential reinforcement of polymer composites. Carbohydr. Polym. 106, 77–83. https://doi.org/10.1016/j.carbpol.2014.02.016.

Fratoni, G., D'Orazio, D., Barbaresi, L., 2019. Acoustic comfort in a worship space made of cross-laminated timber. Build. Acoust. 26, 121–138. https://doi.org/10.1177/1351010X19826250.

Fratoni, G., D'Orazio, D., Barbaresi, L., Garai, M., Cappellini, L., 2023. Mixing materials in false ceilings to increase sound diffusion in education spaces. INTER-NOISE NOISE-CON Congr. Conf. Proc. 265, 5002–5006. https://doi.org/10.3397/IN_2022_0723.

García-Ortuño, T., Andréu-Rodríguez, J., Ferrández-García, M.T., Ferrández-Villena, M., Ferrández-García, C.E., 2011. Evaluation of the physical and mechanical properties of particleboard made from giant reed (*Arundo donax* L.). BioResources 6, 477–486. https://doi.org/10.15376/biores.6.1.477-486.

Gaspar, F., Bakatovich, A., Davydenko, N., Joshi, A., 2020. Building insulation materials based on agricultural wastes. In: Pachecol, T.F., Volodymyr, I., Tsang, D.C.W. (Eds.), Bio-Based Materials and Biotechnologies for Eco-Efficient Construction. Elsevier, pp. 149–170. https://doi.org/10.1016/B978-0-12-819481-2.00008-8.

Ginestet, S., Aschan-Leygonie, C., Bayeux, T., Keirsbulck, M., 2020. Mould in indoor environments: the role of heating, ventilation and fuel poverty. A French perspective. Build. Environ. 169, 106577 https://doi.org/10.1016/j.buildenv.2019.106577.

Glé, P., Gourdon, E., Arnaud, L., 2011. Acoustical properties of materials made of vegetable particles with several scales of porosity. Appl. Acoust. 72, 249–259. https://doi.org/10.1016/j.apacoust.2010.11.003.

Gupta, N., 2019. An analysis of acoustic treatment on recording studio. Int. Res. J. Eng. Technol. 6, 915–920.

Gürü, M., Karabulut, A.F., Aydın, M.Y., Bilici, İ., 2015. Processing of fireproof and high temperature durable particleboard from rice husk. High. Temp. Mater. Process. 34, 599–604. https://doi.org/10.1515/htmp-2014-0092.

Horoshenkov, K.V., Swift, M.J., 2001. The acoustic properties of granular materials with pore size distribution close to log-normal. J. Acoust. Soc. Am. 110, 2371–2378. https://doi.org/10.1121/1.1408312.

EN IEC 60268–16:2020, 2020. Sound system equipment Part 16: Objective rating of speech intelligibility by speech transmission index, European Committee for Electrotechnical Standardization. Geneva, Switzerland.

Ingessil, https://www.ingessil.com/it (last accessed 06.27.23).

ISO 10534–2:2001, 2001. Acoustics - Determination of Sound Absorption Coefficient and Impedance in Impedance Tubes. International Organization for Standardization. Geneva, Switzerland.

ISO 24353:2008, 2008. Hygrothermal performance of building materials and products - Determination of moisture adsorption/desorption properties in response to humidity variation. International Organization for Standardization. Geneva, Switzerland.

ISO 3382–3:2012, 2012. Acoustics -Measurement of room acoustic parameters Part 3: Open plan offices. International Organization for Standardization. Geneva, Switzerland.

ISO 9053–2:2020, 2020. Acoustics - Determination of airflow resistance. Part 2: Alternating airflow method. International Organization for Standardization. Geneva, Switzerland.

Jámbor, A., Török, Á., 2019. The economics of Arundo donax - A systematic literature review. Sustainability (Switzerland) 11. ⟨https://doi.org/10.3390/su11154225⟩.

Johansson, P., Lång, L., Bok, G., Capener, C.M., 2020. Threshold values for mould growth: critical moisture level of 21 different building materials. E3S Web Conf. 172, 1–6. https://doi.org/10.1051/e3sconf/202017220002.

Jones, D., Kržišnik, D., Hočevar, M., Zagar, A., Humar, M., Popescu, C.M., Popescu, M.C., Brischke, C., Nunes, L., Curling, S.F., Ormondroyd, G., Sandberg, D., 2022. Evaluation of the effect of a combined chemical and thermal modification of wood though the use of bicine and tricine. Forests 13. https://doi.org/10.3390/f13060834.

Kinnane, O., Reilly, A., Grimes, J., Pavia, S., Walker, R., 2016. Acoustic absorption of hemp-lime construction. Constr. Build. Mater. 122, 674–682. https://doi.org/10.1016/j.conbuildmat.2016.06.106.

Koizumi, T., Tsujiuchi, N., Adachi, A., 2002. The development of sound absorbing materials using natural bamboo fibers. High. Perform. Struct. Mater. 4, 157–166.

Krejsová, J., Doleželová, M., 2019. Resistance of mortars with gypsum, lime and composite binders against molds. Acta Polytech. CTU Proc. 21, 16–20. https://doi.org/10.14311/APP.2019.21.0016.

Lee, S.H., Md Tahir, P., Lum, W.C., Tan, L.P., Bawon, P., Park, B., Osman Al Edrus, S.S., Abdullah, U.H., 2020. A review on citric acid as green modifying agent and binder for wood. Polymers 12, 1692. https://doi.org/10.3390/polym12081692.

Lee, S.J., Thole, V., 2018. Investigation of modified water glass as adhesive for wood and particleboard: mechanical, thermal and flame retardant properties. Eur. J. Wood Wood Prod. 76, 1427–1434. https://doi.org/10.1007/s00107-018-1324-x.

Liuzzi, S., Sanarica, S., Stefanizzi, P., 2017. Use of agro-wastes in building materials in the Mediterranean area: a review. Energy Procedia 126, 242–249. https://doi.org/10.1016/j.egypro.2017.08.147.

Liuzzi, S., Rubino, C., Stefanizzi, P., Petrella, A., Boghetich, A., Casavola, C., Pappalettera, G., 2018. Hygrothermal properties of clayey plasters with olive fibers. Constr. Build. Mater. 158, 24–32. https://doi.org/10.1016/j.conbuildmat.2017.10.013.

Liuzzi, S., Rubino, C., Martellotta, F., Stefanizzi, P., Casavola, C., Pappalettera, G., 2020a. Characterization of biomass-based materials for building applications: the case of straw and olive tree waste. Ind. Crops Prod. 147, 112229 https://doi.org/10.1016/j.indcrop.2020.112229.

Liuzzi, S., Rubino, C., Stefanizzi, P., Martellotta, F., 2020b. Performance characterization of broad band sustainable sound absorbers made of almond skins. Materials 13, 5474. https://doi.org/10.3390/ma13235474.

Mahieu, A., Alix, S., Leblanc, N., 2019. Properties of particleboards made of agricultural by-products with a classical binder or self-bound. Ind. Crops Prod. 130, 371–379. https://doi.org/10.1016/j.indcrop.2018.12.094.

Malheiro, R., Ansolin, A., Guarnier, C., Fernandes, J., Amorim, M.T., Silva, S.M., Mateus, R., 2021. The potential of the reed as a regenerative building material—characterisation of its durability, physical, and thermal performances. Energies 14. https://doi.org/10.3390/en14144276.

Maraldi, M., Molari, L., Regazzi, N., Molari, G., 2016. Method for the characterisation of the mechanical behaviour of straw bales. Biosyst. Eng. 151, 141–151. https://doi.org/10.1016/j.biosystemseng.2016.09.003.

Maraldi, M., Molari, L., Regazzi, N., Molari, G., 2017. Analysis of the parameters affecting the mechanical behaviour of straw bales under compression. Biosyst. Eng. 160, 179–193. https://doi.org/10.1016/j.biosystemseng.2017.06.007.

Martellotta, F., Cannavale, A., De Matteis, V., Ayr, U., 2018. Sustainable sound absorbers obtained from olive pruning wastes and chitosan binder. Appl. Acoust. 141, 71–78. https://doi.org/10.1016/j.apacoust.2018.06.022.

Martínez-García, C., González-Fonteboa, B., Carro-López, D., Pérez-Ordóñez, J.L., 2020. Mussel shells: a canning industry by-product converted into a bio-based insulation material. J. Clean. Prod. 269. https://doi.org/10.1016/j.jclepro.2020.122343.

Mathews, J.M., Vivek, B., Charde, M., 2023. Thermal insulation panels for buildings using recycled cardboard: experimental characterization and optimum selection. Energy Build. 281, 112747 https://doi.org/10.1016/j.enbuild.2022.112747.

Mati-Baouche, N., De Baynast, H., Lebert, A., Sun, S., Lopez-Mingo, C.J.S., Leclaire, P., Michaud, P., 2014. Mechanical, thermal and acoustical characterizations of an insulating bio-based composite made from sunflower stalks particles and chitosan. Ind. Crops Prod. 58, 244–250. https://doi.org/10.1016/j.indcrop.2014.04.022.

Mati-Baouche, N., de Baynast, H., Michaud, P., Dupont, T., Leclaire, P., 2016. Sound absorption properties of a sunflower composite made from crushed stem particles and from chitosan bio-binder. Appl. Acoust. 111, 179–187. https://doi.org/10.1016/j.apacoust.2016.04.021.

Molari, L., Maraldi, M., Molari, G., 2017. Non-linear rheological model of straw bales behavior under compressive loads. Mech. Res. Commun. 81, 32–37. https://doi.org/10.1016/j.mechrescom.2017.02.010.

Molari, L., Coppolino, F.S., García, J.J., 2021. Arundo donax: a widespread plant with great potential as sustainable structural material. Constr. Build. Mater. 268, 121143 https://doi.org/10.1016/j.conbuildmat.2020.121143.

Muizniece, I., Blumberga, D., 2016. Thermal conductivity of heat insulation material made from coniferous needles with potato starch binder. Energy Procedia 95, 324–329. https://doi.org/10.1016/j.egypro.2016.09.014.

Muñoz Velasco, P., Mendívil, M.A., Morales, M.P., Muñoz, L., 2016. Eco-fired clay bricks made by adding spent coffee grounds: a sustainable way to improve buildings insulation. Mater. Struct. 49, 641–650. https://doi.org/10.1617/s11527-015-0525-6.

Nadhari, W.N.A.W., Danish, M., Nasir, M.S.R.M., Geng, B.J., 2019. Mechanical properties and dimensional stability of particleboard fabricated from steam pre-treated banana trunk waste particles. J. Build. Eng. 26, 100848 https://doi.org/10.1016/j.jobe.2019.100848.

Ng, C.W., Yip, M.W., Lai, Y.C., 2018. The study on the effects of sodium silicate on particleboard made from sugarcane bagasse. Mater. Sci. Forum 911 MSF 66–70. https://doi.org/10.4028/www.scientific.net/MSF.911.66.

Ntimugura, F., Vinai, R., Harper, A., Walker, P., 2020. Mechanical, thermal, hygroscopic and acoustic properties of bio-aggregates – lime and alkali - activated insulating composite materials: a review of current status and prospects for miscanthus as an innovative resource in the South West of England. Sustain. Mater. Technol. 26, e00211 https://doi.org/10.1016/j.susmat.2020.e00211.

Nunes, L., Réh, R., Barbu, M.C., Walker, P., Thomson, A., Maskell, D., Knapic, S., Bajraktari, A., Greef, J.M., Brischke, C., Mansour, E., Ormondroyd, G.A., Teppand, T., Palumbo, M., Lacasta, A.M., 2017. Nonwood bio-based materials. In: Performance of Bio-Based Building Materials. Elsevier, pp. 97–186. https://doi.org/10.1016/B978-0-08-100982-6.00003-3.

O'Flaherty, F., Alam, M., 2021. Thermal and sound insulation performance assessment of vacuum insulated composite insulation panels for building façades. Adv. Build. Energy Res. 15, 270–290. https://doi.org/10.1080/17512549.2018.1520645.

Othmani, C., Taktak, M., Zain, A., Hantati, T., Dauchez, N., Elnady, T., Fakhfakh, T., Haddar, M., 2017. Acoustic characterization of a porous absorber based on recycled sugarcane wastes. Appl. Acoust. 120, 90–97. https://doi.org/10.1016/j.apacoust.2017.01.010.

Owodunni, A.A., Lamaming, J., Hashim, R., Taiwo, O.F.A., Hussin, M.H., Mohamad Kassim, M.H., Bustami, Y., Sulaiman, O., Amini, M.H.M., Hiziroglu, S., 2020. Adhesive application on particleboard from natural fibers: a review. Polym. Compos. 41, 4448–4460. https://doi.org/10.1002/pc.25749.

Palumbo, M., Lacasta, A.M., Holcroft, N., Shea, A., Walker, P., 2016. Determination of hygrothermal parameters of experimental and commercial bio-based insulation materials. Constr. Build. Mater. 124, 269–275. https://doi.org/10.1016/j.conbuildmat.2016.07.106.

Panyakaew, S., Fotios, S., 2011. New thermal insulation boards made from coconut husk and bagasse. Energy Build. 43, 1732–1739. https://doi.org/10.1016/j.enbuild.2011.03.015.

Park, J.H., Kang, Y., Lee, J., Chang, S.J., Wi, S., Kim, S., 2019. Development of wood-lime boards as building materials improving thermal and moisture performance based on hygrothermal behavior evaluation. Constr. Build. Mater. 204, 576–585. https://doi.org/10.1016/j.conbuildmat.2019.01.139.

Pennacchio, R., Savio, L., Bosia, D., Thiebat, F., Piccablotto, G., Patrucco, A., Fantucci, S., 2017. Fitness: sheep-wool and hemp sustainable insulation panels. Energy Procedia 111, 287–297. https://doi.org/10.1016/j.egypro.2017.03.030.

Pina dos Santos, C., Matias, L., 2006. ITE 50. Coeficientes de transmissão térmica de elementos da envolvente dos edifiícios. LNEC.

Platt, S.L., Walker, P., Maskell, D., Shea, A., Bacoup, F., Mahieu, A., Zmamou, H., Gattin, R., 2023. Sustainable bio & waste resources for thermal insulation of buildings. Constr. Build. Mater. 366, 130030 https://doi.org/10.1016/j.conbuildmat.2022.130030.

Posani, M., Veiga, R., de Freitas, V.P., 2021. Retrofitting historic walls: feasibility of thermal insulation and suitability of thermal mortars. Heritage 4, 2009–2022. https://doi.org/10.3390/heritage4030114.

Posani, M., Veiga, R., de Freitas, V.P., 2022. Thermal mortar-based insulation solutions for historic walls: an extensive hygrothermal characterization of materials and systems. Constr. Build. Mater. 315, 125640 https://doi.org/10.1016/j.conbuildmat.2021.125640.

Posani, M., Veiga, R., Freitas, V., 2023. Post-Insulating traditional massive walls in Southern Europe: a moderate thermal resistance can be more effective than you think. Energy Build. 295, 113299 https://doi.org/10.1016/j.enbuild.2023.113299.

Ramos, A., Briga-Sá, A., Pereira, S., Correia, M., Pinto, J., Bentes, I., Teixeira, C.A., 2021. Thermal performance and life cycle assessment of corn cob particleboards. J. Build. Eng. 44, 102998 https://doi.org/10.1016/j.jobe.2021.102998.

Ranesi, A., Posani, M., Veiga, R., Faria, P., 2022. A Discussion on winter indoor hygrothermal conditions and hygroscopic behaviour of plasters in Southern Europe. Infrastructures 7, 38. https://doi.org/10.3390/infrastructures7030038.

Raut, S.P., Ralegaonkar, R.V., Mandavgane, S.A., 2011. Development of sustainable construction material using industrial and agricultural solid waste: A review of waste-create bricks. Constr. Build. Mater. 25, 4037–4042. https://doi.org/10.1016/j.conbuildmat.2011.04.038.

Rey, R.Del, Alba, J., Arenas, J.P., Sanchis, V.J., 2012. An empirical modelling of porous sound absorbing materials made of recycled foam. Appl. Acoust. 73, 604–609. https://doi.org/10.1016/j.apacoust.2011.12.009.

Ricciardi, P., Belloni, E., Merli, F., Buratti, C., 2021. Sustainable panels made with industrial and agricultural waste: thermal and environmental critical analysis of the experimental results. Appl. Sci. 11, 494. https://doi.org/10.3390/app11020494.

Rode, C., Peuhkuri, R.H., Mortensen, L.H., Hansen, K.K., Time, B., Gustavsen, A., Ojanen, T., Ahonen, J., Svennberg, K., Arfvidsson, Jesper TotalRode, C., Peuhkuri, R.H., Mortensen, L.H., Hansen, K.K., Time, B., Gustavsen, A., Ojanen, T., Ahonen, J., Svennberg, K., Arfvidsson, J.T., 2005. Moisture Buffering of Building Materials Department of Civil Engineering Technical University of Denmark. Technical University of Denmark, Department of Civil Engineering.

Romano, A., Bras, A., Grammatikos, S., Shaw, A., Riley, M., 2019. Dynamic behaviour of bio-based and recycled materials for indoor environmental comfort. Constr. Build. Mater. 211, 730–743. https://doi.org/10.1016/j.conbuildmat.2019.02.126.

Rubino, C., Liuzzi, S., Stefanizzi, P., Martellotta, F., 2023. Characterization of sustainable building materials obtained from textile waste: from laboratory prototypes to real-world manufacturing processes. J. Clean. Prod. 390, 136098 https://doi.org/10.1016/j.jclepro.2023.136098.

Sakthivel, S., Senthil Kumar, S., Melese, B., Mekonnen, S., Solomon, E., Edae, A., Abedom, F., Gedilu, M., 2021. Development of nonwoven composites from recycled cotton/polyester apparel waste materials for sound absorbing and insulating properties. Appl. Acoust. 180, 108126 https://doi.org/10.1016/j.apacoust.2021.108126.

Sam-Brew, S., Smith, G.D., 2015. Flax and Hemp fiber-reinforced particleboard. Ind. Crops Prod. 77, 940–948. https://doi.org/10.1016/j.indcrop.2015.09.079.

Sanjay, M.R., Madhu, P., Jawaid, M., Senthamaraikannan, P., Senthil, S., Pradeep, S., 2018. Characterization and properties of natural fiber polymer composites: a comprehensive review. J. Clean. Prod. 172, 566–581. https://doi.org/10.1016/j.jclepro.2017.10.101.

Savic, A., Antonijevic, D., Jelic, I., Zakic, D., 2020. Thermomechanical behavior of bio-fiber composite thermal insulation panels. Energy Build. 229, 110511 https://doi.org/10.1016/j.enbuild.2020.110511.

Savio, L., Pennacchio, R., Patrucco, A., Manni, V., Bosia, D., 2022. Natural fibre insulation materials: use of textile and agri-food waste in a circular economy perspective. Mater. Circ. Econ. 4, 6. https://doi.org/10.1007/s42824-021-00043-1.

Schiavi, A., Guglielmone, C., Miglietta, P., 2011. Effect and importance of static-load on airflow resistivity determination and its consequences on dynamic stiffness. Appl. Acoust. 72, 705–710. https://doi.org/10.1016/j.apacoust.2011.03.009.

Selvaraj, S., Jeevan, V., Rao Jonnalagadda, R., Nishad Fathima, N., 2019. Conversion of tannery solid waste to sound absorbing nanofibrous materials: a road to sustainability. J. Clean. Prod. 213, 375–383. https://doi.org/10.1016/j.jclepro.2018.12.144.

Solt, P., Konnerth, J., Gindl-Altmutter, W., Kantner, W., Moser, J., Mitter, R., van Herwijnen, H.W.G., 2019. Technological performance of formaldehyde-free adhesive alternatives for particleboard industry. Int. J. Adhes. Adhes. 94, 99–131. https://doi.org/10.1016/j.ijadhadh.2019.04.007.

Song, L., Liu, W., Xin, F., Li, Y., 2021. Study of adhesion properties and mechanism of sodium silicate binder reinforced with silicate fume. Int. J. Adhes. Adhes. 106, 102820 https://doi.org/10.1016/j.ijadhadh.2021.102820.

Stefanowski, B.K., Curling, S.F., Ormondroyd, G.A., 2017. A rapid screening method to determine the susceptibility of bio-based construction and insulation products to mould growth. Int. Biodeterior. Biodegrad. 116, 124–132. https://doi.org/10.1016/j.ibiod.2016.10.025.

Tang, X., Zhang, X., Zhang, H., Zhuang, X., Yan, X., 2018. Corn husk for noise reduction: robust acoustic absorption and reduced thickness. Appl. Acoust. 134, 60–68. https://doi.org/10.1016/j.apacoust.2018.01.012.

Trobiani Di Canto, J.A., Malfait, W.J., Wernery, J., 2023. Turning waste into insulation – a new sustainable thermal insulation board based on wheat bran and banana peels. Build. Environ. 5, 110740 https://doi.org/10.1016/j.buildenv.2023.110740.

Tudor, E.M., Kristak, L., Barbu, M.C., Gergel', T., Němec, M., Kain, G., Réh, R., 2021. Acoustic properties of larch bark panels. Forests 12, 1–14. https://doi.org/10.3390/f12070887.

ISO 14125:1998 +A1:2011, 2011. Fibre-reinforced plastic composites -Determination of flexural properties. International Organization for Standardization. Geneva, Switzerland.

UNI 11842:2021, 2021. Bamboo - Determination of the physical and mechanical properties of bamboo culms. Ente italiano di normazione. Milano, Italy.

Verdier, T., Coutand, M., Bertron, A., Roques, C., 2014. A review of indoor microbial growth across building materials and sampling and analysis methods. Build. Environ. 80, 136–149. https://doi.org/10.1016/j.buildenv.2014.05.030.

Vestaeco, 2022, ⟨http://www.vestaeco.com/produkt_VestaEco_INTERNAL,11.html⟩ (last accessed 03.16.22).

Viel, M., Collet, F., Lanos, C., 2018. Chemical and multi-physical characterization of agro-resources' by-product as a possible raw building material. Ind. Crops Prod. 120, 214–237. https://doi.org/10.1016/j.indcrop.2018.04.025.

Viel, M., Collet, F., Lanos, C., 2019. Development and characterization of thermal insulation materials from renewable resources. Constr. Build. Mater. 214, 685–697. https://doi.org/10.1016/j.conbuildmat.2019.04.139.

Voronina, V., Horoshenkov, K., 2004. Acoustic properties of unconsolidated granular mixes. Appl. Acoust. 65, 673–691. https://doi.org/10.1016/j.apacoust.2003.12.002.

Yüksel, N., 2016. The review of some commonly used methods and techniques to measure the thermal conductivity of insulation materials. In: Insulation Materials in Context of Sustainability. InTech, p. 13. https://doi.org/10.5772/64157.